AGU PUBLICATIONS

JGR

Journal of Geophysical Research: Atmospheres

RESEARCH ARTICLE

10.1002/2013JD019771

Special Section:
Volcanism and the Atmosphere

A comparison of satellite- and ground-based measurements of SO_2 emissions from Tungurahua volcano, Ecuador

Brendan T. McCormick[1,2], Michael Herzog[3], Jian Yang[3], Marie Edmonds[2], Tamsin A. Mather[4], Simon A. Carn[5], Silvana Hidalgo[6], and Baerbel Langmann[7]

[1]Department of Mineral Sciences, Smithsonian Institution, National Museum of Natural History, Washington, District of Columbia, USA, [2]Department of Earth Sciences, University of Cambridge, Cambridge, UK, [3]Department of Geography, University of Cambridge, Cambridge, UK, [4]Department of Earth Sciences, University of Oxford, Oxford, UK, [5]Department of Geological and Mining Engineering and Sciences, Michigan Technological University, Houghton, Michigan, USA, [6]Institut für Geophysik, Instituto Geofisico de la Escuela Politecnica Nacional, Quito, Ecuador, [7]Institut für Geophysik, Universitat Hamburg, Hamburg, Germany

Key Points:
- Space-based monitoring of volcanic degassing
- Comparison of satellite- and ground-based data

Supporting Information:
- Readme
- Figure S1

Correspondence to:
B. T. McCormick,
mccormickb@si.edu

Citation:
McCormick, B. T., M. Herzog, J. Yang, M. Edmonds, T. A. Mather, S. A. Carn, S. Hidalgo, and B. Langmann (2014), A comparison of satellite- and ground-based measurements of SO_2 emissions from Tungurahua volcano, Ecuador, *J. Geophys. Res. Atmos.*, *119*, 4264–4285, doi:10.1002/2013JD019771.

Received 8 MAR 2013
Accepted 27 FEB 2014
Accepted article online 6 MAR 2014
Published online 7 APR 2014

Abstract Satellite-measured SO_2 mass loadings and ground-based measurements of SO_2 emission rate are not directly comparable, with ~40% differences between mean emissions reported by each technique from Tungurahua volcano, Ecuador, during late 2007. Numerical simulations of postemission processing and dispersal of Tungurahua's SO_2 emissions enable more effective comparison of ground- and satellite-based SO_2 data sets, reducing the difference between them and constraining the impact of plume processing on satellite SO_2 observations. Ground-based measurements of SO_2 emission rate are used as the model input, and simulated SO_2 mass loadings are compared to those measured by the Ozone Monitoring Instrument (OMI). The changing extent of SO_2 processing has a significant impact on daily variation in SO_2 mass loading for a fixed volcanic emission rate. However, variations in emission rate at Tungurahua are large, suggesting that overall volcanic source strength and not subsequent processing is more likely to be the dominant control on atmospheric mass loading. SO_2 emission rate estimates are derived directly from the OMI observations using modeled SO_2 lifetime. Good agreement is achieved between both observed and simulated mass loadings (~21%) and satellite-derived and ground-measured SO_2 emission rates (~18%), with a factor of 2 improvement over the differences found by simple direct comparison. While the balance of emission source strength and postemission processing will differ between volcanoes and regions, under good observation conditions and where SO_2 lifetime is ~24 hours, satellite-based sensors like OMI may provide daily observations of SO_2 mass loading which are a good proxy for volcanic source strength.

1. Introduction

The measurement of persistent sulphur dioxide (SO_2) gas emissions is a cornerstone of volcano monitoring. Low concentrations of SO_2 in the background atmosphere and its distinctive spectral signatures in both ultraviolet (UV) and infrared (IR) enable much easier detection using remote sensing methods than more abundant volcanic volatiles such as water (H_2O) or carbon dioxide (CO_2) [*Edmonds*, 2008; *Oppenheimer et al.*, 2011]. Measurements of SO_2 afford insight into the storage and release of volatiles from magmas and hence the dynamical and chemical controls on volcanic eruptions, making the monitoring of SO_2 a key component of volcanic hazard mitigation and potential eruption forecasting [*Symonds et al.*, 1994; *Edmonds*, 2008; *Galle et al.*, 2010; *Oppenheimer et al.*, 2011]. Quantification of volcanic SO_2 emission budgets on regional to global scales is also important to understand the role of volcanoes in large-scale cycling of volatiles between Earth's mantle and atmosphere [*Andres and Kasgnoc*, 1998; *Mather et al.*, 2006; *Fischer*, 2008; *Wallace and Edmonds*, 2011; *Mori et al.*, 2013] and the impact of emitted gases on Earth's atmosphere, climate, terrestrial ecosystems, and human population over various spatial and temporal scales [*Robock*, 2000; *Delmelle*, 2003; *Hansell and Oppenheimer*, 2004; *IPCC*, 2007; *Schmidt et al.*, 2012].

Despite a wealth of sensitive remote sensing techniques with which to measure SO_2 emissions (for a recent review, see *Oppenheimer et al.* [2011, and references therein]), persistent degassing into the troposphere at the great majority of volcanoes worldwide is rarely or never monitored due to the prohibitive costs of installing and maintaining ground-based instrument networks in remote and poorly accessible locations [*Sparks et al.*, 2012]. A potential solution is the use of satellite-based spectrometers, which are becoming

increasingly sensitive to atmospheric SO_2 concentrations. One such instrument is the Finnish-Dutch built UV spectrometer OMI (Ozone Monitoring Instrument), which flies aboard NASA's Aura spacecraft in the A-train satellite constellation as part of the Earth Observation System (EOS) mission [*Levelt et al.*, 2006a, 2006b; *NASA*, 2010]. To make full use of such sensors for monitoring volcanic degassing, we must aim to understand and quantify their sensitivity to SO_2 in the troposphere and the accuracy of their measurements.

1.1. Assessing OMI as a Tool for Volcano Monitoring

Since its launch in late 2004, OMI has provided a daily datastream of atmospheric SO_2 column concentrations with near global coverage (note that since late 2008 this coverage has been reduced as a result of the so-called OMI Row Anomaly, http://www.knmi.nl/omi/research/product/rowanomaly-background.php). OMI's combination of a nadir spatial resolution of $13 \times 24\ km^2$ and high spectral resolution in the UV-2 channel (307–383 nm) used for SO_2 retrievals offers unprecedented sensitivity to SO_2 for a satellite-based sensor [*Carn et al.*, 2013]. OMI was the first satellite instrument for which a publicly available online archive of operational SO_2 vertical column densities (VCD) was provided, avoiding the need for a volcanologist user to perform retrievals on the level 1 UV radiance data set. The data can be visualized on the Global Sulphur Dioxide Monitoring homepage (http://so2.gsfc.nasa.gov/), can be downloaded from the Goddard Earth Sciences Data and Information Services Centre (GES DISC, http://disc.sci.gsfc.nasa.gov/), and can be plotted with a set of IDL routines, collectively called OMIPLOT (*Carn* [2011], downloadable from https://vhub.org/resources/682).

The OMI data set has enabled many new contributions to volcanology and the space-based remote sensing of SO_2 emissions, including the following: the identification and characterization of major but previously poorly known volcanic sources of SO_2 [*Bani et al.*, 2009a, 2009b; *McCormick et al.*, 2012], as well as major anthropogenic sources [*Carn et al.*, 2007b; *NASA*, 2008]; new arc-scale surveys assessing the relative strength and persistence of multiple active volcanoes and linking trends in observed SO_2 to volcanic activity [*Carn et al.*, 2008; *Carn and Prata*, 2010; *Bani et al.*, 2012; *McCormick et al.*, 2012]; detection of eruptions at remote or unmonitored volcanoes [*Carn et al.*, 2009b; *Ferguson et al.*, 2010; *Gardine et al.*, 2011; *Carn et al.*, 2013]; and tracking of drifting SO_2 eruption clouds for aviation hazard mitigation [*Carn et al.*, 2009a; *Thomas et al.*, 2011].

It is noteworthy, however, that "monitoring" of gas emission is typically taken to mean regular (often daily) quantitative assessment of the amount of SO_2 being released by a volcano. It is currently not widely accepted that OMI (or any other satellite-based sensor) truly has this capability. Long-term total arc-scale SO_2 emissions budgets calculated from OMI data for Ecuador [*Carn et al.*, 2008], Vanuatu [*Bani et al.*, 2012] and Papua New Guinea [*McCormick et al.*, 2012] appear consistently to be large underestimates (~40%) relative to those calculated from ground-based measurements. The limited volcanology-related validation of the OMI SO_2 product which exists either focuses on opportunistic studies of drifting eruption clouds in the upper troposphere/lower stratosphere (UTLS) [*Spinei et al.*, 2010; *Carn and Lopez*, 2011; *Lopez et al.*, 2013] rather than persistent lower intensity degassing into the free troposphere or planetary boundary layer or is inconclusive due to measured SO_2 concentrations falling very close to the instrument's detection limit [*Carn et al.*, 2011].

Major uncertainties limiting the interpretation of OMI data require further investigation, including the following: the impact of widely variable detection limits with altitude, latitude, and season [*Carn et al.*, 2013]; a range of factors impacting observation conditions such as meteorological cloud cover, the OMI row anomaly, heavy plume ash loadings, and off-nadir viewing geometries [*McCormick et al.*, 2013]; and, perhaps most importantly, the impact of atmospheric processing on SO_2 mass prior to satellite overpass and measurement. SO_2 can be oxidized to sulphate (SO_4^{2-}) through both homogeneous and heterogeneous processes. In the gas phase, oxidation occurs by reaction with hydroxyl radicals ($OH^{\bullet}$), while aqueous-phase oxidation involves reaction with H_2O_2 and O_3 [*Saxena and Seigneur*, 1987; *Seigneur and Saxena*, 1988; *Eatough et al.*, 1994]. Although measurements of these reactions in volcanic plumes are sparse, studies of industrial smokestacks suggest that very rapid conversion rates of SO_2 ($> 10\%\ h^{-1}$) can be achieved [*Eatough et al.*, 1994]. SO_2 can also be removed from the atmosphere by dry deposition and undergo advective transport by prevailing winds. Determining whether changes in daily SO_2 mass loading are the result of the variable extent of this postemission modification, as opposed to changes in volcanic source strength (i.e., SO_2 emission rate), is an essential step toward the use of satellite data sets in monitoring volcanic degassing.

1.2. Integrating Ground- and Satellite-Based Gas Data Sets

Direct comparison between data sets obtained from satellite- and ground-based measurements is complicated by their distinct approaches. Ground-based data sets typically comprise SO_2 emission rates measured with differential optical absorption spectroscopy (DOAS) by miniature UV spectrometers [*Edmonds et al.*, 2003; *Galle et al.*, 2010; *Oppenheimer et al.*, 2011]. Measurements are made close to the volcano (within a few kilometers of the vent) and shortly after emission (frequently <1 h). Fresh volcanic plumes are poorly mixed and highly heterogeneous, and this method samples this heterogeneity with a very different degree of averaging to satellite-based measurements, often made across much greater spatial scales (typical footprints are several km^2). Additionally, ground-based automatic scanning spectrometers measure gas emissions continuously over a period of several hours and hence may observe a range of degassing behavior. UV satellite instruments with a single daily overpass are limited to a near-instantaneous snapshot of atmospheric SO_2 mass loading, though observations of older gas plumes downwind are also possible. Several hours may intervene between emission of volcanic gas and its measurement by local ground-based instruments, and the subsequent overpass and observation by a satellite-based instrument. During this time extensive chemical reaction, physical deposition processes, and plume transport and dilution may reduce (or disperse below detection) the mass of SO_2 in the volcanic cloud. If satellites are to play a role in the monitoring of volcanic degassing—and their use offers the great advantage of regular observations on a global scale—these issues must be overcome or at least be better understood.

Some earlier studies have "derived" SO_2 emission rate from satellite observations of SO_2 mass loading, with the aim of a more representative comparison with ground-based data sets. Various methods have been developed, each best suited to particular conditions. *Lopez et al.* [2013] demonstrated the "scene lifetime method" using airborne measurements of wind speed and OMI observations of plume length to estimate SO_2 lifetime in the tropospheric plume of Redoubt volcano, Alaska. Emission rates were then derived using the generic residence time equation:

$$Q = \frac{M}{\tau} \tag{1}$$

where Q is SO_2 emission rate, M is SO_2 mass loading, and τ is SO_2 lifetime, which is estimated from independently observed wind speed under the assumption of a steady state balance between SO_2 emission and removal [*Carn et al.*, 2013; *Lopez et al.*, 2013]. This approach is appropriate for elongate linear plumes without significant bifurcation, whose length in the direction of overall downwind transport can easily be gauged, allowing SO_2 lifetime to be estimated. Estimating emission rates from discrete drifting clouds of SO_2, perhaps resulting from minor explosive eruptions, are not well suited to this approach. *Lopez et al.* [2013] showed strong correlation between satellite- and ground-based estimates of SO_2 emission rate, though OMI estimates were consistently lower than those of the ground-based DOAS instruments.

Where other data are available to constrain SO_2 lifetime, a broader range of plume geometries can be considered since there is no need to evaluate the OMI scene in the lifetime calculation. Later in this article, we use SO_2 lifetimes calculated from Regional Model with Tracer Extension (REMOTE) model simulations to derive emission rates from OMI-measured mass loadings, the "model lifetime method." Similarly, direct measurements (e.g., of downwind changes in SO_2 column density) could be used to evaluate atmospheric lifetime and applied to the emission rate calculations.

An alternative method, termed the "transect method," is analogous to ground-based or airborne spectrometer measurements, where integrated SO_2 concentrations in the plume cross section are multiplied by wind speed to either reconstruct a time series of emission rate or provide enough values to calculate a representative average [*Merucci et al.*, 2011; *Campion et al.*, 2012; *Carn et al.*, 2013]. This requires a high resolution wind data set, and although it can be used for near-vent measurements, OMI's coarse spatial resolution (specifically the effect of spatially averaging a subpixel plume) limits the accuracy of these estimates compared to those from satellite instruments such as ASTER.

More recently, *Carn et al.* [2013] presented a method of deriving emission rate from a single OMI pixel, again assuming steady state conditions between input of SO_2 to the pixel and its removal solely by advection; this method is a development of that described by *Ichoku and Kaufman* [2005] to calculate aerosol emissions from MODIS observations of biomass burning. This method requires detailed knowledge of the wind field also, particularly the relative direction of the wind to the orientation of the OMI pixel in question. The method works best where a plume is confined to a single pixel and so can be used very close to source and

also where the assumption of advection-only removal is more likely to be valid, such as in cloud-free scenes with long SO_2 lifetimes (e.g., high latitudes).

This study compares ground- and satellite-based measurements of persistent lower intensity SO_2 degassing at Tungurahua volcano, Ecuador, in order to further evaluate OMI for volcano monitoring. We use a regional-scale atmospheric chemistry/transport model, REMOTE, to aid the comparison of satellite- and ground-based SO_2 emissions data sets as well as investigating the impact of atmospheric processing on OMI observations of SO_2. We use REMOTE to simulate the postemission fate of SO_2 released from Tungurahua volcano, in terms of oxidation, deposition, and transport of SO_2. Tungurahua was chosen since its emissions have been previously studied with OMI observations as well as ground-based data sets [*Carn et al.*, 2008; *Arellano et al.*, 2008] and measurements of SO_2 emission using ground-based spectrometers that continue to the present day. The use of a chemistry/transport model allows a bridging of the gap in time which separates ground-based measurements of Tungurahua's SO_2 emission rate (used here as the model input) from the atmospheric column densities (or mass loadings) ultimately measured by OMI, which are compared with simulated SO_2 column densities (the model's output). The mismatch in spatial resolution between the two data sets is also avoided by this method.

The idea of model/satellite comparison studies in volcanology is gaining increasing currency. Recent studies by *Haywood et al.* [2010] and *Heard et al.* [2012] compared satellite- and ground-based measurements of atmospheric SO_2 and sulphate concentrations with dispersion model simulations for explosive eruptions, including Sarychev Peak, Eyjafjallajökull, and Kasatochi. *Boichu et al.* [2013] and *Theys et al.* [2013] used combinations of inverse modeling with various satellite SO_2 products to reconstruct SO_2 emission rate time series for the eruptions of Eyjafjallajökull, Puyehue-Cordón Caulle, Nabro, and Nyamulagira. Our work complements these earlier studies due to our focus on persistent, quasi-passive emissions into the free troposphere rather than sporadic eruptions, and our aim is to assess the potential for satellite-based monitoring of continuous emissions such as these.

2. Tungurahua Volcano

Tungurahua (1.476°S, 78.442°W) is a large (5023 m high) andesitic stratovolcano and one of the most active volcanoes in Ecuador [*Siebert and Simkin*, 2002]. Sustained eruptions have occurred roughly once per century, for the past ~1300 years [*Hall et al.*, 1999]. The current eruption (1999 to present) is characterized by the alternation of explosive Vulcanian and Strombolian episodes with periods of lower intensity gas, steam, and minor ash emissions [*Arellano et al.*, 2008]. Larger subplinian and plinian eruptions occurred in July and August 2006, respectively [*Steffke et al.*, 2010]. Tungurahua's activity has included pyroclastic flows, lava flows, lahars, and tephra and ash falls, so it is considered a major hazard to around 25,000 people in the surrounding area as well as to the Agoyán hydroelectric dam, to the northeast of the volcano [*Hall et al.*, 1999]. Drifting volcanic clouds from explosive eruptions pose a potentially serious threat to the aviation community [*Steffke et al.*, 2010]. Monitoring of the volcano is performed by the Instituto Geofísico de la Escuela Politécnica Nacional (IGEPN), with seismological, geochemical, thermal, geodetic, acoustic, and other observational techniques overseen from the Observatorio del Volcán Tungurahua (Figure 1).

Smithsonian Institution weekly reports (available online at http://volcano.si.edu/) provide brief summaries of activity at Tungurahua during our study period of October to November 2007 and are themselves drawn from IGEPN observatory reports (available online at http://www.igepn.edu.ec/informes/volcanicos.html, Spanish only). Tungurahua's activity during October to November 2007 largely consisted of continuous gas and steam emissions, accompanied by ash venting explosive eruptions of varying intensity. IGEPN categorize this interval as part of a longer period of explosive eruptive activity, beginning on 1 October 2007 and persisting until 10 February 2008; the only deviation from this to a period of nonexplosive eruptive activity is defined as 6–11 October, where daily explosions fell to zero or one (Figure 3d). The level of detail between daily reports is inconsistent, but the overall pattern is comparable throughout, with frequent ashfall around the volcano, plume heights varying between 5 and 9 km altitude, and frequent explosions recorded by IGEPN's seismometer network. The number of daily explosions might be used as a proxy for intensity of activity, though until 10 November when 64 were reported, the daily total never exceeds 25. Following this date, the total explosions remained below 30 per day, until the final 5 days of the study period (25–30 November) when 77, 185, 116, 162, and 133 explosions, respectively, were reported (Figure 3d). The observatory reports describe a period of sustained inflation measured by tiltmeters from 4 to 21 October, which

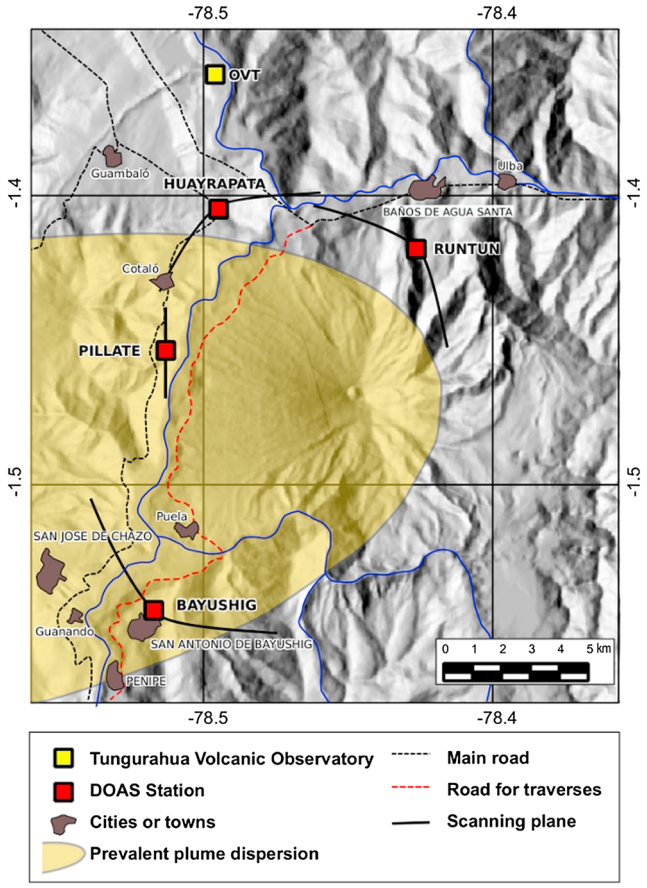

Figure 1. Tungurahua volcano and environs, overlain on a Digital Elevation Model basemap generated from the Instituto Geográfico Militar topography data set, showing prevalent plume dispersion, location of notable habitations and infrastructure, and the position of the volcano observatory and UV spectrometer (DOAS) stations.

was then followed by significant deflation and higher reported gas emissions (reflected in higher mean SO_2 emissions measured by ground-based UV DOAS spectrometers in November rather than October—see following section). The interpretation suggested in the IGEPN reports is of a shallow magma intrusion, which produced increased seismicity and degassing but did not lead to a major eruption, in contrast to the August 2006 eruption [*IGEPN*, 2007a, 2007b, 2007c].

3. REMOTE Simulations

REMOTE (Regional Model with Tracer Extension) was developed in order to simulate the postemission dispersal and processing of a range of natural and anthropogenic trace gas and aerosol emissions [*Langmann*, 2000] and has already been applied to volcanic SO_2 emissions in Indonesia [*Pfeffer et al.*, 2006] and Nicaragua [*Langmann et al.*, 2009]; other studies have simulated volcanic ash transport, forest fire emissions, and anthropogenic pollution [*Marmer and Langmann*, 2005; *Langmann et al.*, 2010; *Pfeffer et al.*, 2012; *O'Dowd et al.*, 2012].

REMOTE combines the physics of the earlier regional climate model REMO, with added tropospheric chemistry [*Langmann et al.*, 2009; *Pfeffer et al.*, 2012]. Trace gases can undergo a range of chemical reactions and in addition be removed from the model domain by either transport processes or wet/dry deposition. Gas-phase chemistry is based on the RADM II model [*Stockwell et al.*, 1990]. Since emissions from anthropogenic and natural sources are not available in the spatial resolution necessary for the chosen study, photooxidant precursor concentrations (e.g., NO and CO) are prescribed as constant background concentrations. This enables the model to reasonably simulate the diurnal cycle of photooxidants like $OH^{\bullet}$ and H_2O_2 which are important for sulphate formation. Oxidation of SO_2 to sulphate can occur by both gas- and aqueous-phase reactions, though their relative contribution is not explicitly distinguished

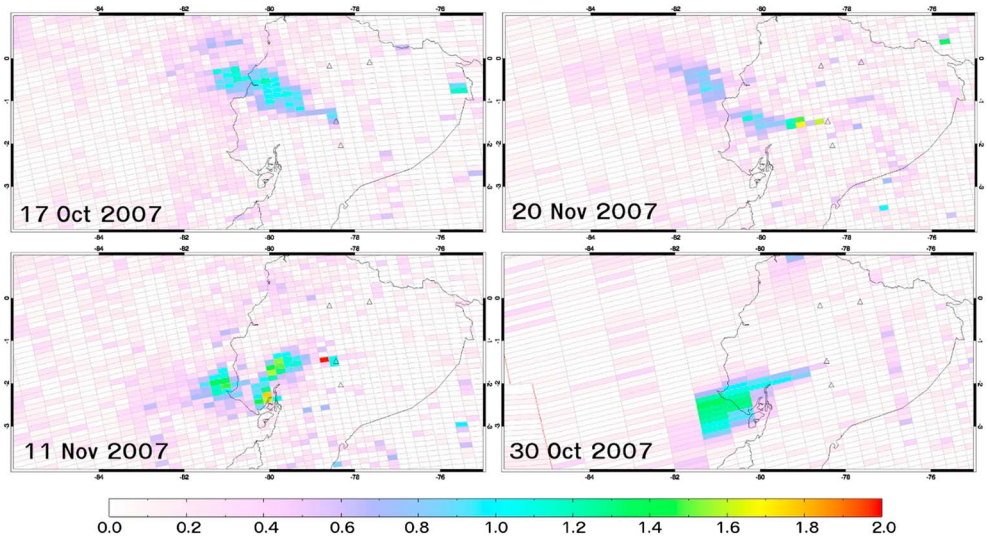

Figure 2. Selected representative OMI SO_2 plume maps (footprint plots), with SO_2 column density in Dobson units (1 DU = 2.69×10^{16} molecules cm^{-2} and 0.02848 g SO_2 m^{-2}). Maps from 17 October and 20 November 2007 show plumes interpreted as quasi-passive degassing, where emissions have merged into a single coherent linear plume. Map from 11 November shows a similar situation, but three evident SO_2 maxima within the plume extent are interpreted as evidence of minor explosive eruptions which release semidiscrete clouds of higher SO_2 mass. Map from 30 October is interpreted to represent OMI's observation of a larger explosive eruption.

in the model's output. Physical transport processes modeled include horizontal and vertical advection [*Smolarkiewitz*, 1983], vertical transport in convective cloud [*Tiedtke*, 1989], and vertical turbulent diffusion [*Mellor and Yamada*, 1974]. To ensure that the meteorological conditions do not continue to deviate over the course of the simulation, all meteorological data are reinitialized every 24 h from European Centre for Medium-Range Weather Forecasts (ECMWF) reanalysis data, whereas chemistry and tracer transport are simulated continuously.

In this study, the REMOTE model setup is similar to that in *Langmann et al.* [2009]. REMOTE uses 40 vertical layers between the Earth's surface and the 10 hPa pressure level, ~32 km altitude. The horizontal resolution is 0.1° (~10 km), which is finer than OMI's nadir footprint. The model domain (75–86°W and 4°S–1°N) extends westward from central Ecuador over the Pacific Ocean and encompasses the typical extent of Tungurahua's SO_2 plumes, based on OMI daily scenes. The horizontal resolution of 10 km results in a certain degree of topographic smoothing, with the height of the volcano being underestimated. SO_2 injection altitude was fixed at 7 km, which is considered representative of reported SO_2 plume height during the study interval. Validation of REMOTE's ability to produce local metereological conditions was demonstrated by *Langmann et al.* [2009] via comparison with satellite-based precipitation and wind speed data sets.

4. SO_2 Emissions Data Sets

4.1. OMI Observations of SO_2

SO_2 plumes originating from Tungurahua are consistently observed by OMI (http://so2.gsfc.nasa.gov/, *Carn et al.* [2008]), which is attributed to the volcano's persistent and relatively high long-term mean SO_2 emission [*Arellano et al.*, 2008] and OMI's relatively low SO_2 detection limits (~ 30–60 $\times$ 10^3 kg SO_2) in low latitudes and midtropospheric altitudes (>5 km) [*Carn et al.*, 2013]. *Carn et al.* [2008] showed that trends in a 2 year time series of daily SO_2 mass loadings over Tungurahua could be related to changing intensity of eruptive activity, including the waning and waxing of consecutive eruption cycles, and long-term increasing SO_2 emission prior to the major explosive eruptions of July and August 2006. Significant variation in plume SO_2 mass and geometry can be seen in daily OMI scenes, and these can be interpreted to reflect different states of activity, such as continuous, quasi-passive degassing or more pulsed emission associated with explosive activity (Figure 2). Discrete drifting clouds with central SO_2 column density maxima tend to represent earlier explosively released SO_2 emissions, while elongate plumes with their maximum SO_2 pixel over the volcano typically reflect persistent degassing with decreasing SO_2 column density downwind. Attempts to correlate interpretations of activity based on visual inspection of OMI scenes with available daily IGEPN

observatory reports proved unsuccessful: none of the days mentioned above with particularly high numbers of explosions corresponded to OMI scenes with obvious discrete drifting SO_2 clouds. Overall, 16 daily OMI scenes were interpreted as indicating mostly explosive SO_2 release, while the remaining 43 showed more continuous plumes.

The OMI data used in this study is operational Level 2 OMSO2 data derived from Level 1 radiances with the linear fit (LF) algorithm of *Yang et al.* [2007]. The retrieved SO_2 column densities were calculated assuming the SO_2 layer's center of mass altitude (CMA) lies at 7.5 km; plume heights during the study period area were reported as 5–9 km altitude, so this is considered reasonable. Based on the high altitude of Tungurahua's summit and the volcano's topographic prominence, we make the assumption that the plume will always enter the free troposphere rather than become trapped in the boundary layer. A study region between 75–86°W and 4°S–1°N was defined based on maximum observed plume extents in daily OMI scenes, and daily SO_2 mass loadings were calculated using OMIplot routines. All daily scenes were inspected for contributing emissions from other volcanoes nearby: Reventador lies near the northern margin of the domain, but no significant plumes were observed during the study period, and no drifting SO_2 clouds from eruptions elsewhere traversed the domain. The apparent SO_2 mass loading over a similar-sized domain offshore to the west which was unaffected by the plume was calculated and subtracted from each daily mass loading over the study region in order to correct for background noise.

4.1.1. Errors and Uncertainties

Error analysis of the operational OMI SO_2 product is the focus of ongoing investigation and difficult to express quantitatively. For optimum viewing conditions (low cloud fraction, free tropospheric plume without significant ash content, and low solar zenith angle) where the altitude of the SO_2 plume is accurately known, retrieval errors are chiefly determined by radiative transfer calculation errors and those arising due to noise in the instrument's radiance measurements and should be <5% [*Carn et al.*, 2013]. However, such a scenario is rarely encountered. In this study, the main potential sources of error we identify are uncertain or variable SO_2 plume altitude, potentially widespread cloud cover, and increases in plume opacity arising from higher ash contents during explosive intervals at Tungurahua.

The assumed 7.5 km SO_2 plume CMA is considered valid for the majority of Tungurahua's emissions, with SO_2 mass loadings in plumes at lower or higher altitudes, respectively, being overestimated or underestimated, respectively, by ~10% for the variation in plume altitude reported (5–9 km). Under clear sky conditions, linear scaling may be used to adjust retrieved SO_2 VCDs for changes in plume altitude [*Carn et al.*, 2013], though this is not attempted here since reliable plume altitude estimates are not available on a daily basis at Tungurahua.

Tungurahua experiences persistent and widespread cloud cover due to its equatorial location and humid atmosphere, with weather systems typically arriving from the rainforested region to the east, based on prevailing easterly winds. OMI measurements of reflectivity over a domain considered representative of typical SO_2 plume location are a good proxy for cloud fraction and can be plotted alongside daily OMI SO_2 mass observations (Figures 3a and 3b). While we note generally high cloud fractions (reflectivity is mostly ~30–60%, mean = 47%), there is only limited evidence from this plot for reduced OMI mass loadings coinciding with peaks in cloud fraction, for example, on 7 October and 4, 7, 17, and 30 November; other peaks do not coincide with reduced SO_2 mass loading. Visual inspection of OMI daily scenes can also aid assessment of cloud interference: composite plots of SO_2 mass loading and reflectivity are suggestive of cloud cover obscuring the volcano on 12 and 19 October as well as 4 and 30 November (see http://so2.gsfc.nasa.gov/). We suggest that due to the high altitude of SO_2 injection from Tungurahua, OMI SO_2 plumes are generally emplaced above the cloud deck rather than below. In this case, errors would be reduced due to the higher reflectivity of the cloud tops increasing backscatter of UV radiation. This is clearly a broad assumption, however, and we note that while 10–20% errors in the LF retrieval algorithm are estimated for interference by subpixel meteorological cloud [*Yang et al.*, 2007], this error may increase dramatically with cloud fraction [*Carn et al.*, 2013]. A comparison of SO_2 mass loadings retrieved assuming plume CMAs of 2.5 km and 7.5 km show reasonable linear correlation ($r^2 = 0.81$), which we consider sound evidence for only limited cloud interference in the retrievals (Figure 3).

The impact of ash on the LF retrieval is not well quantified, and we make no assessment of this potential error here. While Tungurahua is prone to regular minor explosive eruptions, we anticipate that the ash

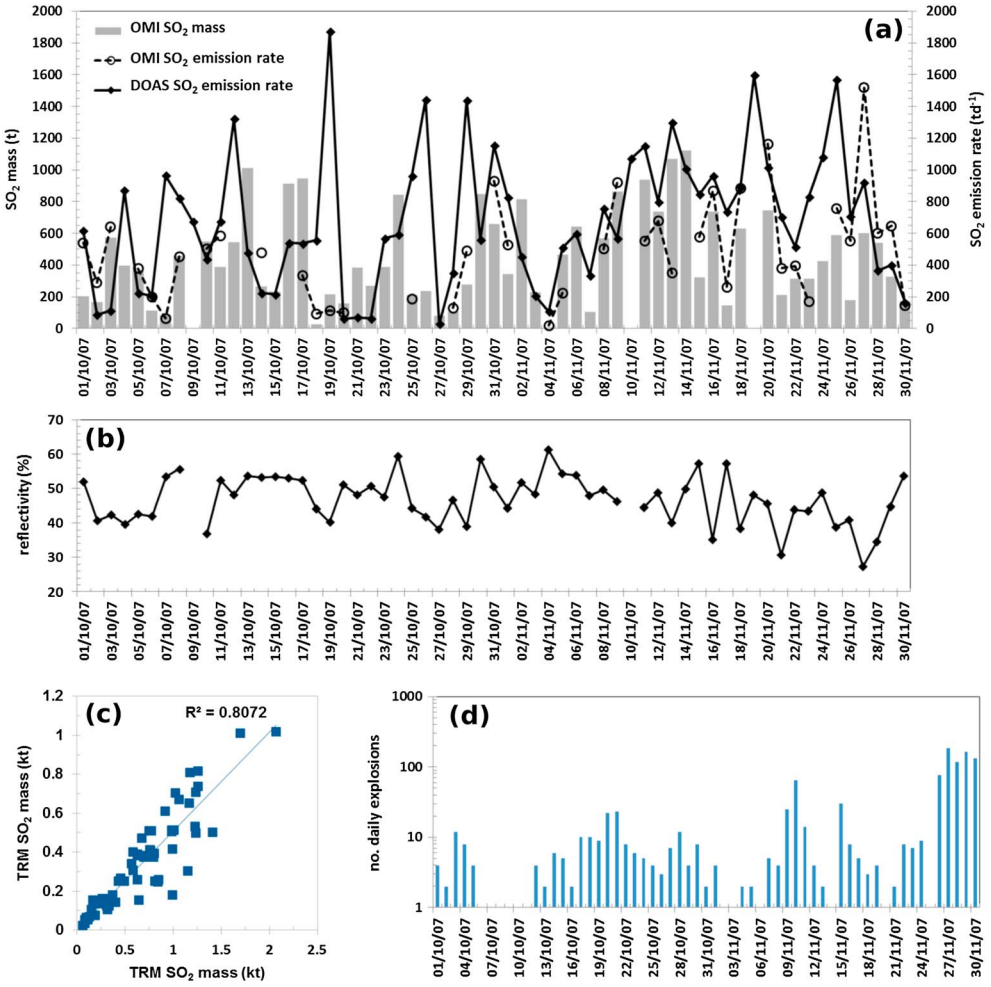

Figure 3. (a) Time series of daily SO_2 mass loading measured by OMI and mean daily SO_2 emission rate measured by ground-based DOAS and derived using *scene lifetime method* from coincident OMI observations. Gaps in the OMI data set indicate the instrument's twice-monthly day of operation in so-called zoom mode [*Levelt et al.*, 2006a, 2006b]; note that error bars of 23% for OMI and 42% for DOAS are omitted for clarity; (b) time series of OMI-observed daily mean scene reflectivity for plume pixels; (c) comparison of SO_2 mass loading data sets where the lower troposphere (TRL) and medium troposphere (TRM) retrievals are used; (d) time series of daily explosions reported at Tungurahua in IGEPN reports; may be considered a crude proxy for plume ash content.

loading for these is unlikely to be major for significant quantities to remain in the plume for long periods of time.

A final consideration is that changing OMI viewing geometry through the satellite's orbital cycle may impact column density and mass loading estimates [*Lopez et al.*, 2013]. The instrument's swath is binned into 60 pixel rows in the cross-track direction, which increase in size off-nadir to a maximum of $24 \times 160\,km^2$. Increasing viewing angle therefore corresponds to a loss of spatial resolution, which can preclude the detection of smaller SO_2 plumes or contribute to underestimates in mass loading. Plume extents and margin may also be poorly constrained relative to near-nadir viewing scenes. SO_2 plumes were observed at particularly large viewing angles on 2, 11, 18, and 27 October and 3, 12, 19, and 28 November, and these days must therefore be interpreted with caution.

Overall, by calculating total error as the square root of the sum of each individual error squared, we estimate each daily OMI SO_2 mass loading to be subject to ~23% error. We note that this estimate is likely to be a minimum due to the uncertain impacts of increased cloud fraction, potential for ash in the plume, and days where the plume lies at the edge of OMI's swath. The error on derived emission rate estimates (see discussion below) will also be slightly larger due to error on the wind speed data used.

4.2. Ground-Based Measurements of SO_2 Emissions

IGEPN have monitored SO_2 emissions from Tungurahua since 1998, initially using a correlation spectrometer (COSPEC), and post-2004 using automatic scanning UV DOAS instruments [*Arellano et al.*, 2008]. The mean daily SO_2 emission rate during 1999–2006 was 1458×10^3 kg day^{-1}, with a standard deviation of 2026×10^3 kg day^{-1}, reflecting the significant variability in degassing between more eruptive versus more quiescent phases of activity [*Arellano et al.*, 2008] as well as errors in the emission rate calculation resulting from poorly constrained wind speed, for example. In 2007, a new network of scanning DOAS instruments was installed at Tungurahua through the NOVAC program [*Galle et al.*, 2010]; there are presently four spectrometers at four stations on the volcano's flanks (Figure 1). During our study period of October and November 2007, three instruments were operational at Bayushig, Huayrapata, and (for the final few days only) Pillate stations. Each instrument makes several tranverse scans of the plume during daylight hours, with an emission rate calculated after each complete scan by multiplying the measured integrated SO_2 concentration in the plume cross section with wind speed in the direction of transport. These near-real-time measurements of emission are typically averaged to estimate a daily mean value. We identified the most representative daily mean emission rate estimate to be from that station which met at least two of the following criteria: (1) where the highest value of SO_2 emission rate was calculated; (2) which was closest to the plume; and (3) which had the most complete scans of the full extent of the plume. From this selection a composite time series of SO_2 emission rate throughout October to November 2007 was obtained (Figure 3). We note that these selection criteria have the potential to contribute to some overestimation of emission rates, especially on days where the plume may be particularly close to one station.

4.2.1. Errors and Uncertainties

The error in ground-based UV DOAS measurements of SO_2 emission rates arises from combined errors in spectroscopy, measurement geometry, atmospheric scattering, and wind parameters [*Kern*, 2009; *Galle et al.*, 2010].

Errors associated with the DOAS retrieval itself, spectrometer stray light, and with temperature effects are generally small (<10%) [*Kern*, 2009] and have been well characterized experimentally [*Galle et al.*, 2010]. The major error related to measurement geometry is plume height. While plume height can be calculated trigonometrically from simultaneous plume observations by two instruments, this remains relatively rare operationally, and estimates of this kind are not routinely made at Tungurahua. Instead, plume height is fixed at 5 km, i.e., vent altitude, which is likely to be an underestimate of true plume height, particularly on days characterized by more explosive activity. Without a reliable daily plume height data set, this error is difficult to quantify. The generic error schemes for DOAS measurements of volcanic plumes described by *Kern* [2009] and *Galle et al.* [2010] suggest 15–40% as a potential range.

Uncertain wind direction and speed are the most widely discussed sources of error in SO_2 emission rate data sets. Plumes which make a perpendicular intersection with an instrument's scanning plane result in negligible error, while deviations of 90° from the perpendicular result in 100% error [*Kern*, 2009]. In selecting data from one station per day, we were able to avoid using any data from days where intersection angles were > 45° from perpendicular. *Arellano et al.* [2008] suggested 10% error results from deviations of 30° from perpendicular, which is likely to be reasonably appropriate for this study.

Reliable wind speed data sets are required to assess plume speed, a key parameter in emission rate calculations. Operationally within the NOVAC network, wind data comes from global models; at Tungurahua the data used are the ECMWF ERA-Interim reanalysis data set [*Dee et al.*, 2011]. Future strategies might include direct calculation of plume speed from DOAS measurements [*Galle et al.*, 2010; *Boichu et al.*, 2010; *Williams-Jones et al.*, 2006], but these are not yet widely in routine use. The value of wind speed and direction for the model grid point closest to the location of Tungurahua is noted once per day, being selected as the one of four daily model updates closest in time to the hours of measurement. The spatial resolution of the model (14×16 km^2) precludes account being taken of local topographically induced variations in wind speed, which may significantly affect calculated SO_2 emission rates [*Nadeau and Williams-Jones*, 2009]. The average speed and direction of the wind data used in calculation of the IGEPN SO_2 emission rate data set used in this study agree closely with both a 7 year (1999–2006) measured wind speed data set reported near Tungurahua [*Arellano et al.*, 2008] and the long-term average provided by NCEP-DOE Reanalysis 2 data (accessed via *Palma*'s [2013] Wind Reanalysis tool, available online at https://vhub.org/resources/windre/). As will be shown later (see Figure 6), there is also broad agreement between ECMWF and REMOTE mean wind speeds, though we note that some differences are to be expected since the two data sets have

different spatial resolution and different representations of topography. *Arellano et al.* [2008] suggest a 30% error arising due to uncertainty in wind speed, which again is considered likely to be appropriate here.

Lastly, much recent work has focussed on two competing radiative-transfer-related effects as potentially major sources of error in published and operational DOAS-measured SO_2 emission rate data sets. Multiple scattering of photons due to particles (e.g., ash, aerosol, and condensed water) within a plume can increase optical path length and overestimate plume SO_2 amounts, while light which has not encountered the plume may be scattered into the instrument field of view, which dilutes the measured absorption signal, effectively underestimating SO_2 plume amounts [*Kern*, 2009; *Galle et al.*, 2010; *Kern et al.*, 2010]. The failure to take account of realistic radiative transfer effects such as these is a major uncertainty in most operational DOAS SO_2 data sets. Recent theoretical and modeling work [*Kern et al.*, 2010] and preliminary field testing [*Kern et al.*, 2012] suggest resulting underestimates in measured emission rates of 20–90%, depending on factors such as SO_2 and aerosol column densities. Further investigation into these effects and their impact on DOAS monitoring of SO_2 emissions is urgently needed but are beyond the scope of this study. *Kern* [2009] proposes that 30% error due to these uncertainties is a reasonable minimum estimate.

Overall, calculating in the same way as for the OMI data set, we estimate a ~42% minimum error on each emission rate value arising from a complete scan of the volcanic plume. This error could be significantly higher on certain days. While subdaily variation in measured emission rate must exceed the bounds of this error to be considered as true variability, it will be seen from the large standard deviation on the daily mean emission rates that we report throughout this paper that high variability within each day is also an important factor to consider when analyzing this data set.

4.3. Direct Comparison of OMI and Ground-Based Data Sets

The complete 2-monthly time series of ground-based measurements of daily mean SO_2 emission rate is shown in Figure 3a, alongside the corresponding daily SO_2 plume mass loadings measured by OMI and other parameters relating to OMI measurements. Noting that emission rates and mass loadings should not, strictly, be directly compared in quantitative terms (see earlier discussions), the generally weak agreement in pattern evident between these data sets demonstrates that increased SO_2 emission rate from Tungurahua does not simply correspond to increased atmospheric SO_2 mass over the volcano detected by OMI. Most notably, none of the sharp peaks in emission rate measured by ground-based DOAS instruments (e.g., 12, 19, 26, and 29 October and 19 and 25 November) correspond to peaks in mass loading. The only interval with reasonable agreement between the ground- and satellite-based data sets is roughly ~3–14 November. The mean SO_2 emission rate from DOAS measurements is 683.7×10^3 kg day^{-1}, while the mean daily SO_2 mass loading measured by OMI is 448.8×10^3 kg. The percentage difference between these two values (percentage difference calculated as difference between two means divided by their average) of 41.5% is comparable to that found in previous comparisons of OMI and ground-based DOAS SO_2 data sets [*Carn et al.*, 2008; *Bani et al.*, 2012; *McCormick et al.*, 2012].

Figure 3 also shows a time series of SO_2 emission rate derived from OMI observations using the *scene lifetime method* [*Carn et al.*, 2013; *Lopez et al.*, 2013], alongside the ground-based data set. Emission rate from a scene is equal to the plume mass multiplied by the plume speed divided by the plume length. Speed was obtained from REMOTE simulated windfields, which due to the better spatial resolution were considered favorable to the reanalysis data sets used by IGEPN at Tungurahua; plume lengths were measured using OMIplot routines. The overall agreement between these two data sets appears to be slightly improved relative to that discussed in the preceding paragraph, though the incompleteness of the derived satellite data set, owing to unsuitable plume geometry on 16 days (11 from October, five from November), precludes any systematic comparison. The sharp peaks in the ground-based data set are again unmatched by corresponding peaks in the satellite data set. The percentage difference, calculated as before, between OMI scene-derived and ground-based DOAS-measured SO_2 emission rate is 35.1%, a slight improvement on the use of mass loadings and emission rates together but still comparable to the previously observed underestimates by OMI.

The extreme peaks in measured SO_2 emission rate, as well as the extremely low values, are difficult to interpret in terms of major changes in volcanic degassing or other activity owing to the inconsistent detail available in observatory reports. It is, in any case, misleading to assume that increases in visible activity or seismic activity, for example, would necessarily correspond to increased SO_2 emission or other simply evident correlation. It is theoretically possible to account for these extreme values by consideration of certain

of the errors in the SO_2 data sets, as discussed above. Increased plume ash content and hence increased opacity could impede effective DOAS or OMI SO_2 retrievals, leading to minima in the retrieved quantity. Equally, however, cloud cover could have the same result, and high plume particle contents could (through multiple scattering) alternatively contribute to overestimations of SO_2 concentrations (and hence mass loadings or emission rates); no correlation, however, was found between daily emission rates and number of explosions, which could be considered a rough proxy for ash in the plume. We also note that our selection criteria for the DOAS data (see section 4.2) is likely to introduce some bias toward higher values, though our use of combined criteria should ensure that no erroneously high values are selected. To seek explanation for these extreme values in such ways remains speculative, and it would not be appropriate to remove days where it was assumed that one particular source of error led to the data being unreliable. At this point, we merely draw attention to this high frequency variability in the data sets and note that in a subsequent section of this article (section 8) we consider time-averaging of the SO_2 emissions data sets as a potential means of suppressing this variability in order to isolate broader underlying patterns.

A longer term and more preferable solution is of course to reduce the errors in each data set. On the ground-based side, the use of direct wind and plume height measurements to complement or replace the current general estimates used (whether informed by regional meteorological models or observations of typical volcanic activity) would significantly reduce uncertainties, as will continuing study into the impact of badly constrained radiative transfer assumptions in the operational DOAS retrieval. Considering OMI, the key uncertainties of subpixel meteorological cloud and plume ash content both require further investigation. In the former case, coincident observations of SO_2 plumes by OMI and cloud maps by another A-train satellite such as MODIS would be an interesting case to pursue.

In summary, direct comparison of daily satellite and ground-based SO_2 data sets, whether using mass loading or emission rate, clearly does not produce convincing agreement. Average values of each data set are different by 35–40%, which is similar to previous studies, as outlined. We explore whether the use of the REMOTE model can facilitate a more effective comparison and potentially reduce these differences.

5. Simulations of SO_2 Plume Dispersion

5.1. Model Output From Runs With Fixed SO_2 Input

REMOTE simulations were performed for October and November 2007, using fixed monthly mean SO_2 emission rates of 604×10^3 kg day^{-1} and 766×10^3 kg day^{-1}, respectively.

A comparison of REMOTE-simulated SO_2 VCD maps to those from OMI observations reveals only limited agreement (Figure 4). In monthly time-averaged maps, SO_2 plumes in both observed and simulated data sets exhibit dominantly westward transport of the volcanic plume and decreasing SO_2 VCDs downwind. REMOTE is able to broadly reproduce both the observed dispersion pattern and magnitude of SO_2 emissions, with more agreement in terms of the latter in November than in October. Plume geometries are rather dissimilar, however, with OMI observed plumes having a more ragged appearance to their margins, often multiple SO_2 maxima, and more prominent bifurcations. These differences arise since REMOTE simulates the constantly ongoing dispersal and processing of a fixed (each month) and continuous SO_2 emission rate from the volcano. OMI observations, however, record more complex dispersal patterns, since they are produced from a series of instantaneous snapshots of the plume and may capture transient explosive events as well as sustained persistent degassing, short-lived perturbations in the general wind field, or particularly thick cloud overlying some or all of the plume. The OMI plume maps effectively have variable SO_2 emission, processing, and viewing conditions convolved together, which can make them difficult to interpret in terms of changing volcanic activity.

The simulated SO_2 plume maps are clearly of little use themselves as a means of validating OMI SO_2 maps, though arguably a more sophisticated simulation with SO_2 emission rate and altitude of injection varying at high frequency (together with the variable meteorology which REMOTE already exhibits) could perhaps approach this. Our aim instead is to explore the variability evident in the simulated SO_2 VCD maps, which results solely from SO_2 processing—the input of SO_2 to the model is fixed, and unlike OMI there are no changing observation conditions to consider. Visual inspection of 10 day time-averaged simulated plume maps (Figure 4) confirms that relatively significant variation in plume dispersion direction, plume geometry, downwind decrease in VCD, and overall magnitude can occur from changes in the combined effects of oxidation, deposition, and transport of SO_2. For example, the 11–20 and 21–31 intervals of October show much

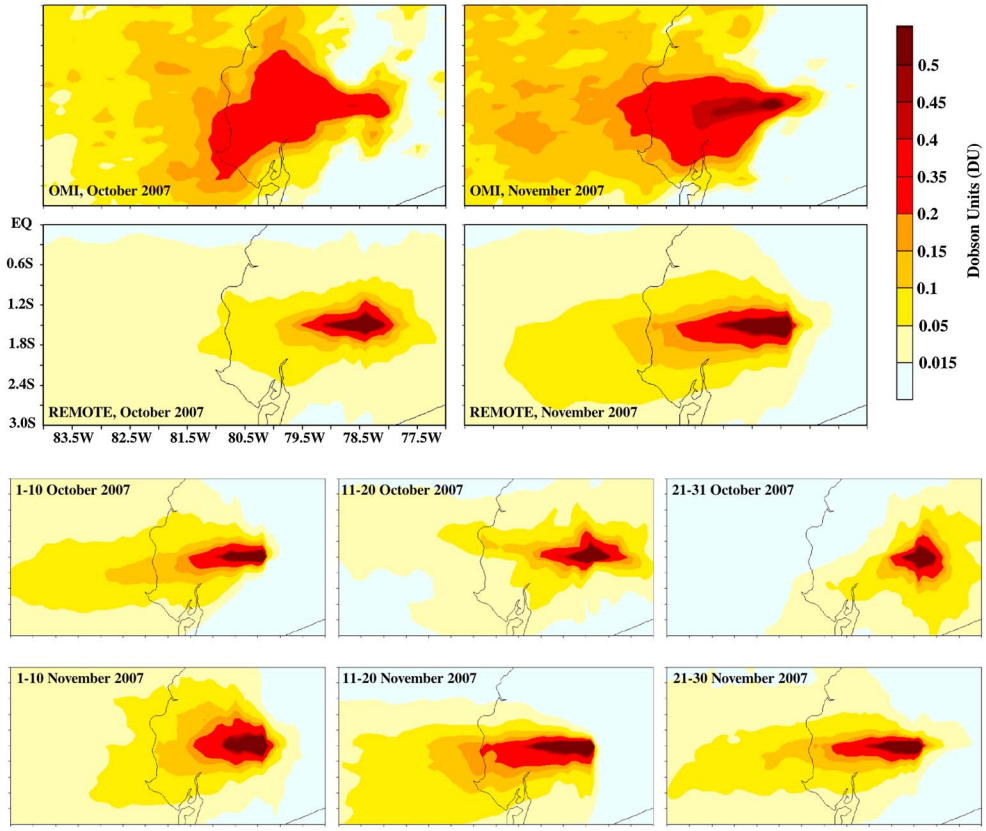

Figure 4. SO_2 vertical column density (VCD) maps from OMI and REMOTE. (top) Monthly means for (left) October and (right) November for each data set, OMI and REMOTE. (bottom) Ten-day mean maps of REMOTE SO_2 VCD for the entire study period. All maps have the same color scale, and the same region is shown in each.

less consistent westward dispersal, as does 1–10 November compared to the rest of the month. Higher VCDs persist for greater distances downwind in 1–10 October and 11–30 November than at other times.

Simulated daily SO_2 mass loadings in October to November 2007 vary between ~400 and 1000 kg $\times 10^3$ kg SO_2 (Figure 5a). When daily mass loading rises above the value of daily input (i.e., monthly mean SO_2 emission rate—shown as a dashed horizontal line in Figure 5a), this indicates that SO_2 is generally retained in the model domain for longer; conversely, when daily mass falls below the value of input, SO_2 removal has a greater influence. Peaks and troughs in the REMOTE SO_2 mass loading time series are thus interpreted as intervals of relatively reduced or increased processing. While there is no strong agreement in trend between the model data set and the OMI observations of SO_2 mass loading, we propose that certain common peaks and troughs (e.g., 16–30 November) may indicate that plume processing does influence the SO_2 mass measured by OMI, at least under some circumstances. Overall mean daily SO_2 mass loading from the simulations is 508×10^3 kg SO_2 and 612×10^3 kg SO_2 for October and November, respectively, compared to 396×10^3 kg SO_2 and 507×10^3 in the OMI data set. This equates to a percentage difference between the data sets of 24.9% and 18.7% in October and November, or 22.0% overall, compared to 42% calculated between mean OMI mass loadings and DOAS emission rates. Throughout the study period, 10 day mean SO_2 mass loadings in the OMI and REMOTE data sets show better agreement than was previously shown between OMI and DOAS data set. The use of the model clearly improves the bulk difference between the satellite and ground-based data sets. Mean SO_2 loadings from OMI observations are closer to those calculated from REMOTE simulations than they are to the mean emission rates calculated from the DOAS data sets (Table 1).

5.2. Recalculating Model Output Based on Variable SO_2 Emission Rate as Input

A more representative comparison between REMOTE simulations and OMI observations of course must account for changes in volcanic emission rate (i.e., source strength). Since the availability of reactant oxidant molecules such as $OH^{\bullet}$ and O_3 in REMOTE is prescribed, in good approximation the model's output,

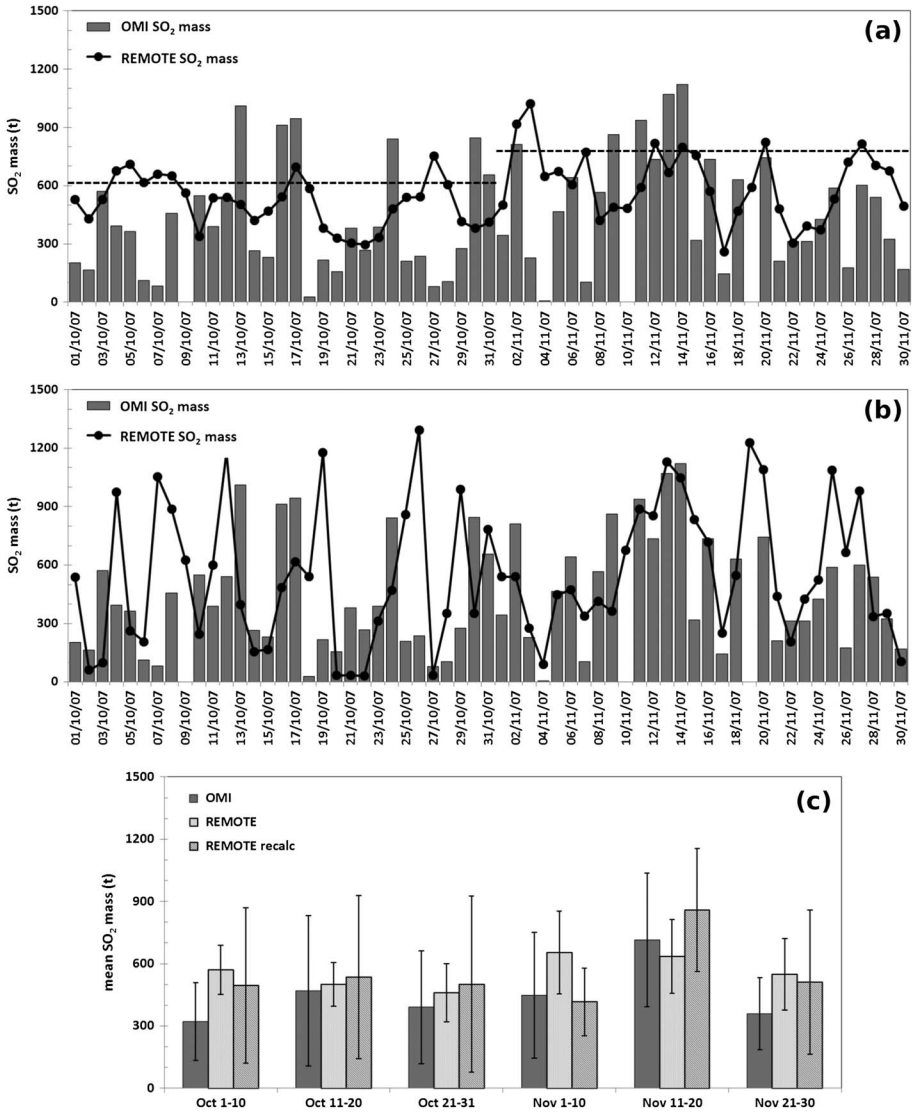

Figure 5. (a) Time series of daily SO_2 mass loading measured by OMI and simulated by REMOTE, October to November 2007. REMOTE simulations are based on a fixed SO_2 input in each month, being the mean SO_2 emission rate measured by DOAS (shown by dashed line, units are kg SO_2 per day). (b) Same time series as in Figure 5a but with REMOTE output scaled by daily DOAS SO_2 emission rate. (c) Bar chart of 10 day time-averaged SO_2 mass loadings, from OMI observations, REMOTE simulations, and recalculated REMOTE simulations. Error bars indicate the standard deviation on each 10 day mean.

SO_2 mass loading, responds linearly to changes in input, SO_2 emission rate. By dividing each simulated daily SO_2 loading in Figure 5a by the monthly mean emission rate and then multiplying by daily mean emission rate (from the ground-based DOAS data set), a new time series can be plotted (Figure 5b) which gives an indication of the combined impact of variable volcanic source strength and variable extent of SO_2 processing.

Following this recalculation, the shape of the REMOTE SO_2 time series changes dramatically, having many more extreme values than the original simulated output. This arises from the highly variable nature of the DOAS-measured SO_2 emission rate data used to calculate the scaling factor. Indeed, the recalculated REMOTE output closely resembles in shape, as we would expect, the DOAS emission rate time series. However, this model time series, being of mass loading rather than emission rate, can be directly compared to the OMI observations, and between these time series at certain points there is clearly better agreement than between either (1) the OMI and ground-based data sets or (2) the OMI and original REMOTE data sets. For example, in the month of November, the shape of the two time series is very similar, with exceptions which

Table 1. Percentage Difference Between Mean SO_2 Emissions From Each Pair of Data Sets for October 2007, November 2007, and the Full Study Interval

	October	November	Overall
OMI SO_2 mass, DOAS SO_2 emission rate	41.63	40.60	41.49
OMI SO_2 mass, REMOTE SO_2 mass	24.89	18.72	21.97
OMI SO_2 mass, REMOTE SO_2 mass (*recalculated*)	25.30	15.98	20.70
OMI SO_2 emission rate (*scene.*), DOAS SO_2 emission rate	50.38	28.22	35.10
OMI SO_2 emission rate (*model.*), DOAS SO_2 emission rate	17.30	17.11	17.63

can often be easily explained, such as the missing OMI data on the days when the instrument was operating in "zoom mode" [*Levelt et al.*, 2006a]. Peaks in the model data set (arising from the underlying peaks in DOAS-measured emission rate) on 20, 25, and 27 November are all unmatched, however, and in addition to these days there are notably large discrepancies between simulations and satellite observations on 1, 7, 15, and 26 November. We note that among these days 15 November had higher than average scene reflectivity (Figure 3b); though this is not the case on the other days cited, it may be that increased cloud cover resulted in some obscuring of the OMI plume.

Agreement in shape of the two time series is worse in October, with very few intervals of more than 1 or 2 days where the two data sets are comparable (the fall and rise between 13 and 17 or increase from 22 to 24 are perhaps the most convincing intervals for a common trend). There are significantly more extreme values in October, again resulting from the underlying ground-based data set. The wide difference between OMI and REMOTE SO_2 mass loadings on 7, 8, and 19 October could conceivably be a result of cloud cover (Figure 3 and earlier discussion), though again this cannot account for any more of the days with some large discrepancies (e.g., 4, 12, 18, 19, 25, 26, and 29 October). Among these latter, the discrepancy on 18 October might result from the large viewing angle of OMI when observing the plume on that day (section 4.1.1), but this explanation offers nothing to the remaining problem days through the entire October to November 2007 period.

Percentage differences were calculated between daily OMI and REMOTE SO_2 mass loadings and plotted against mean scene reflectivity, the number of daily explosions reported by the volcano observatory, and the OMI viewing angle for the pixel with maximum detected SO_2 column density (see supporting information). These comparisons allow assessment of whether cloud fraction, plume ash content, or satellite viewing geometry control agreement between OMI and the ground-based data (represented by REMOTE output). In each case, no correlation was found (r^2 <0.05). This suggests that no single one of these factors contributes dominantly to agreement or lack thereof between satellite and ground-based data sets. Similar conclusions were reported in an earlier comparison of OMI and airborne measurements of tropospheric SO_2 column density [*Lopez et al.*, 2013].

The highly fluctuating nature of both OMI and REMOTE time series (Figure 5) clearly impedes straightforward comparison; the number of uncertainties facing each data set clearly also plays a role. As such it is difficult to unequivocally declare whether the inclusion of volcanic source strength as a variable improves or worsens the overall agreement between OMI observed and REMOTE simulation SO_2 mass loadings. Based on 10 day time-averaged mean SO_2 mass loadings, the satellite and both model data sets agree within uncertainty (standard deviation) (Figure 5). However, the large magnitude of the standard deviation clearly limits the meaningfulness of this result, particularly in the recalculated model data set, where the spread of data approaches 2 orders of magnitude. This large variability may be important evidence in that the forcing of the model output by the changing emission strength is simply greater than that of the forcing by changing processing; further simulations are required to characterize this fully. The OMI data set does not contain high variability to quite the same extent as the recalculated model data set (evidenced by generally smaller standard deviation on the mean values in Figure 5c), and the extreme maxima in SO_2 mass loading do not appear to be readily explainable from comparisons of DOAS emission rate with coincident activity. We suggest that this high variability, together with an increase in similarity of shape between the observed and simulated time series through November, indicates that source strength could prove the strongest control on mass loading. There are no intervals of the time series in Figure 5 where the inclusion of variable source strength clearly decreases agreement between simulated and observed SO_2 mass loading, and on the whole the 10 day mean OMI mass loadings are closer to the REMOTE means after recalculation (Figure 5c). Considering the study period as a whole, the percentage differences between OMI and recalculated REMOTE mean

SO_2 mass loadings are 25.3% and 16.0% in October and November and 20.7% overall (Table 1). This minor improvement over the use of the original REMOTE output is interpreted as evidence that source strength is more important than processing overall, though to a greater extent in November.

6. The Balance in Plume Processing Between Oxidation, Deposition, and Transport

The highly variable SO_2 emission rates measured at Tungurahua (<200×10^3 to >1600×10^3 kg SO_2 per day) may certainly on many days dominate over the lower amplitude variability in SO_2 mass loadings caused by changing processing. We now consider this processing in more detail, namely, which of oxidation of SO_2 to sulphate (SO_4^{2-}), deposition of SO_2, or downwind advective transport of the plume plays the major role in removing SO_2 from the model domain following emission and whether changes in the balance or extent of these three processes might affect the overall impact of processing versus emission strength on SO_2 mass loading. We discuss here the model output from the original simulations (the recalculated data are not appropriate for use here since processing is convolved with variable emission strength).

6.1. Overall Balance in Plume Processing and SO_2 Lifetime

The mean SO_2 emission rate through the study period of October to November 2007 was calculated from DOAS data as 342.0×10^3 kg S day^{-1}. The mean SO_2 mass loading in the REMOTE domain for the same interval was 279.8×10^3 kg S. Dividing this mean loading by mean emission rate provides an estimate of SO_2 lifetime (τ_{SO_2}) in the model domain, 19.6 h. Similarly, we can compute SO_2 lifetimes for each component of processing (oxidation (τ_{oxid}), deposition (τ_{dep}), and transport (τ_{trans})) and relate all of these lifetimes thusly:

$$\frac{1}{\tau_{SO_2}} = \frac{1}{\tau_{oxid}} + \frac{1}{\tau_{dep}} + \frac{1}{\tau_{trans}} \quad (2)$$

Lifetime due to oxidation (τ_{oxid}) can be calculated by dividing the mean SO_2 mass loading (279.8×10^3 kg S) by the mean SO_4^{2-} mass loading (202.1×10^3 kg S) which is equal to the amount of SO_2 removed each day by oxidation. The result is $\tau_{oxid} = 33.3$ h. Since this is much longer than the calculated total lifetime of SO_2 in the model domain, another of the processes must also be reasonably significant to keep the bulk lifetime below 1 day.

Dry deposition of SO_2, essentially comprising the downward fall of SO_2 without influence of rain, appears to be a process of only minor significance at Tungurahua. Mean daily SO_2 dry deposition rates for October to November 2007 were 1.6×10^3 kg S day^{-1}, though sporadic yet significant positive excursions in dry deposition rate (maximum reported 12.0×10^3 kg S day^{-1}, 3 November) result in a standard deviation of 2.0×10^3 kg S day^{-1}. Typically, however, mass of SO_2 removed by dry deposition each day is <1% of total SO_2 mass loading. Therefore, τ_{dep} is very long, equalling 4197.0 h. This slow rate of removal by dry deposition versus oxidation is not surprising, given the warm, humid atmospheric conditions over Tungurahua and the typical emission of SO_2 into the free troposphere rather than the planetary boundary layer.

Transport of SO_2 from the model domain is the final component of processing. A certain component of transported SO_2 (equal to 62.2×10^3 kg S) is the difference between the mean daily input (342.0×10^3 kg S day^{-1}) and the mean daily SO_2 mass loading (279.8×10^3 kg S). Additionally, the difference between SO_2 daily mass loading and the sum of SO_2 removed by oxidation and dry deposition as outlined above equals 76.1×10^3 kg S. Dividing the daily SO_2 mass loading by the sum of these two components of transported SO_2 gives $\tau_{trans} = 48.6$ h and results in a balanced lifetime equation.

6.2. Daily Variation in the Balance of Plume Processing Controls

Our results suggest that oxidation is generally responsible for the removal of 59.1% of the SO_2 from the model domain, with transport responsible for removal of 40.0% and dry deposition being a process of relatively negligible importance (0.9%). This balance is expected to vary between days, according to variable conditions. Figure 6 presents time series of various REMOTE outputs: SO_2/SO_4^{2-} (here and after, we are referring to mass ratio), SO_2 dry deposition flux, and mean wind velocity (for a small subdomain close to the volcano) for October to November 2007, with mean liquid water path plotted alongside SO_2/SO_4^{2-} and ECMWF mean wind velocity plotted alongside REMOTE wind velocity. The simulated SO_2/SO_4^{2-} ratio typically varies within a fairly limited range (mean $\pm$ standard deviation = 1.67 ± 1.0), though three striking peaks are evident (Figure 6a)). Increases in SO_2/SO_4^{2-} are indicative of reduced oxidation of SO_2 (i.e., production of SO_4^{2-}). This must, given a fixed SO_2 input to the model, be due to less favorable conditions for oxidation reactions to take place or that SO_2 is preferentially removed by another process.

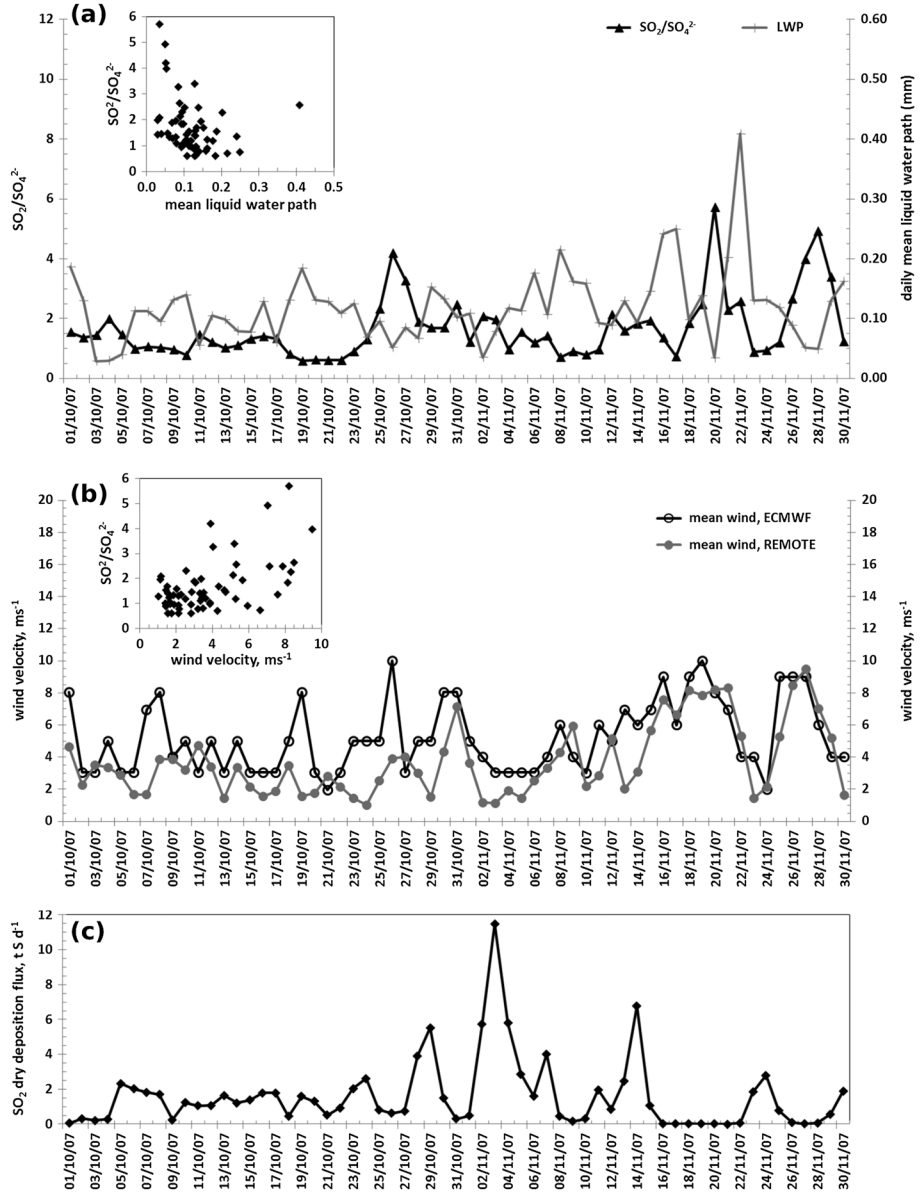

Figure 6. Time series of REMOTE-simulated daily variation in selected parameters related to SO_2 plume processing, October-November 2007, namely, (a) SO_2/SO_4^{2-} ratio and liquid water path, (b) mean wind velocity across a subsection of the model domain close to the volcano (1–2°S, 78–79°W) as well as the ECMWF reanalysis wind data used in DOAS calculations, and (c) SO_2 dry deposition flux.

The model output (SO_4^{2-} mass loading) is not explicitly quantified in terms of what arose from gas-phase oxidation of SO_2 involving photolytic molecules such as $OH^{\bullet}$ versus oxidation in the aqueous phase. However, since model domain $OH^{\bullet}$ concentrations are prescribed in REMOTE, variation in oxidation is more influenced overall by variable water availability: reduced mean liquid water path over the volcano results in reduced oxidation and hence increases in SO_2/SO_4^{2-} (Figure 6a).

Some similarity in shape of the time series between SO_2/SO_4^{2-} and mean wind speed is also evident, with coincident peaks in both toward the end of November (Figures 6a and 6b). This is interpreted as higher wind speeds removing SO_2 faster from the model domain before it can be oxidized. Lastly, despite the aforementioned large increases in dry deposition rate on individual days (Figure 6c), the maximum amount of SO_2 removed by this process remains <5%, and it seems unlikely that dry deposition can significantly affect overall balance in plume processing controls.

Overall, the extent of SO_2 processing simulated by REMOTE appears to vary within relatively narrow margins. Short, pronounced excursions do occur in all three components of plume processing (oxidation, dry deposition, and transport/wind speed), however, and it is plausible that these excursions could more strongly influence SO_2 mass loading on these given days than volcanic source strength does. All of the "excursions" mentioned above occur in November, so it is unlikely that changes in the balance of processing can be a major influence on the agreement between OMI and REMOTE SO_2 mass loadings in October. Of the days identified in November, however, where the greatest discrepancy was seen between these two data sets, some might be interpreted as having experienced significant changes in typical processing. On 20 and 26–28 November, Figure 6 indicates significant peaks in both SO_2/SO_4^{2-} (and hence reduced oxidation) and wind velocity. The former would not be expected to result in an underestimate by OMI relative to the simulated SO_2 mass loading, since both should be positively influenced by a reduction in oxidation of SO_2. However, it is possible that increased wind speed could contribute to an underestimate if shearing were to reduce the apparent column density of SO_2 to OMI's view. Wind velocities began increasing on 15 November and could also account for discrepancies on that day and 17 November, though we note that on 16 and 18 November the two data sets agree closely. Percentage differences between OMI and REMOTE daily SO_2 mass loadings show no correlation (again, r^2 <0.05) with any of SO_2/SO_4^{2-}, mean liquid water path, SO_2 dry deposition, or either measure of wind velocity (see supporting information). This suggests that there is no dominant control by total oxidation, aqueous chemistry, deposition, or transport on the agreement between OMI and REMOTE data sets.

6.3. Comparison of Calculated SO_2 Lifetime With Previous Studies

Even if SO_2 emission rate is considered overall to exert the stronger influence on atmospheric SO_2 mass loading at Tungurahua, short-lived variations in both relative and absolute magnitudes of oxidation or transport processes seem able to alter the balance in favor of a greater processing influence. A bulk SO_2 lifetime of 19.6 h is equal to a typical loss rate (the reciprocal of lifetime) of 1.4×10^{-5} s^{-1}. This value falls squarely within the range of published estimates of SO_2 loss rate in tropospheric volcanic plumes ($\sim 10^{-3}$–10^{-7} s^{-1}) [*Oppenheimer et al.*, 1998; *McGonigle et al.*, 2004; *Rodríguez et al.*, 2008]. Such a wide range, however, invites consideration that in other environments, for example, at a volcano emitting SO_2 into the planetary boundary layer rather than the free troposphere, much faster processing is likely and could therefore have a stronger influence than emission rate the majority of the time. At Soufrière Hills volcano, *Rodríguez et al.* [2008] reported average SO_2 loss rates of $\sim 10^{-4}$ s^{-1}, an order of magnitude faster than what REMOTE simulations suggest for Tungurahua. *Oppenheimer et al.* [1998] reported even faster loss rates exceeding $\sim 10^{-3}$ s^{-1} at Soufrière Hills and Etna volcanoes. We note, however, that in the case of boundary layer plumes, it is OMI's diminished sensitivity to SO_2 (due to greater attenuation of radiation further down in the atmosphere) which is likely to be the limiting factor on measuring SO_2 loadings which accurately reflect true emissions from a volcano [*Carn et al.*, 2013].

Masaya volcano is another whose plume is typically injected into the boundary layer, but during a dry season measurement campaign, *McGonigle et al.* [2004] measured average loss rates of $\sim 10^{-5}$ s^{-1}, comparable to those we calculate here for Tungurahua but significantly slower than those at Soufrière Hills, interpreted as a result of ash-free plumes released into clear skies. The colder and drier high-latitude environments of Erebus, Mount St. Helens, and Redoubt volcanoes are also interpreted as the cause of slower measured loss rates [*Oppenheimer et al.*, 1998]. In settings such as these, where SO_2 lifetime is much longer, it seems more likely that emission rate would be the dominant control on observed SO_2 mass loading. However, similarly to our example of Soufrière Hills, other factors may be more likely to influence OMI observations. Due to high ozone column concentrations and relatively greater thicknesses of atmosphere for photons to pass through (due to higher solar zenith angle), OMI's sensitivity to SO_2 is greatly diminished at higher latitudes, resulting in much higher detection limits [*Lopez et al.*, 2013; *Carn et al.*, 2013; *McCormick et al.*, 2013].

The absence of ash from our simulations is important to note. Ash particles may provide reaction surfaces and cloud seeding nuclei, both of which could significantly increase loss rates. At Tungurahua during our study period, explosive activity did occur, as is testified by observatory reports and visual inspection of daily OMI scenes. However, this sporadic activity was typically mild in intensity and duration, and we do not think there was persistent ash in the plume downwind. Higher ash content immediately following emission is anticipated, though, which points to nonconstant loss rate even on the dimensions of a single SO_2 plume. Constraining this heterogeneity falls beyond the scope of this study.

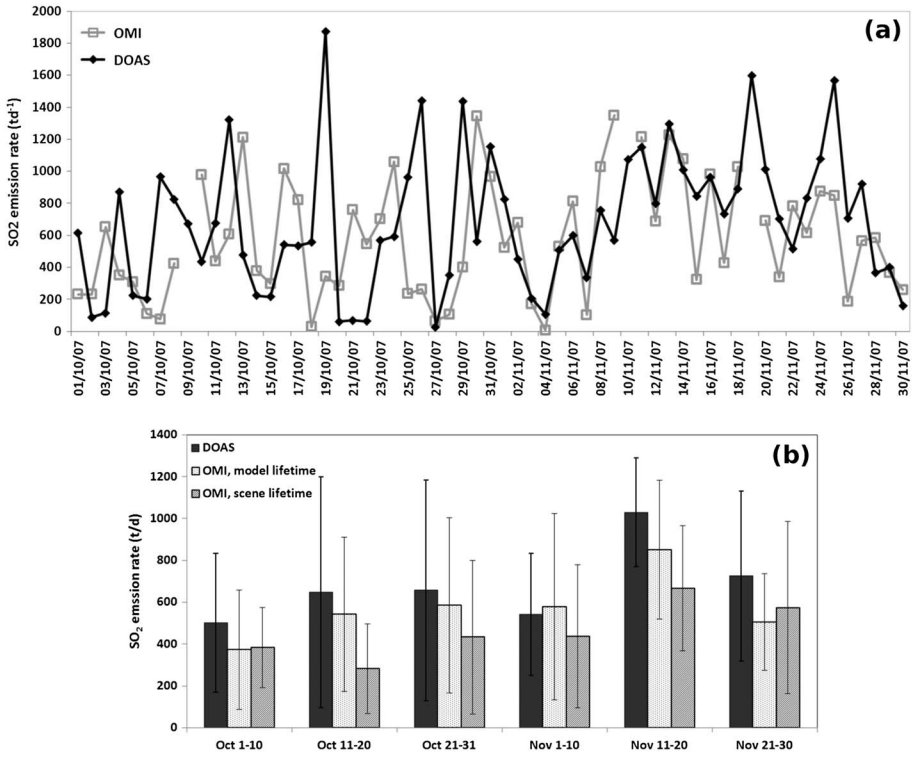

Figure 7. (a) Daily time series of SO_2 emission rate measured by ground-based UV DOAS spectrometers and derived using the *model lifetime method* from coincident OMI observations. (b) Bar chart of 10 day time-averaged SO_2 emission rates from ground-based UV DOAS spectrometer measurements and derived from OMI observations using the *scene lifetime* and *model lifetime* methods. Error bars indicate standard deviation on each mean.

7. Deriving SO_2 Emission Rate From the OMI Mass Loading Data Set

Using REMOTE to calculate tropospheric SO_2 lifetime for each day of October to November 2007, we can derive estimates of SO_2 emission rate directly from the OMI data set, using the SO_2 lifetime method (section 1.2) [*Carn et al.*, 2013; *Lopez et al.*, 2013]. This results in a time series of daily SO_2 emission rate from OMI observations (Figure 7), which provides an additional, more direct method to compare the satellite and ground-based measurements of SO_2 degassing at Tungurahua in addition to our preceding discussion of comparing OMI and REMOTE SO_2 mass loadings. The use of the model lifetime, rather than the scene lifetime demonstrated in section 4.3, results in a much more complete data set, facilitating a more effective comparison. Other potential methods for deriving emission rate (outlined in section 1.2) were not used here owing to a combination of unavailability of wind data sets at sufficiently high spatial resolution, unfavorable OMI plume geometries, and uncertainty over the extent of spatial averaging of subpixel plumes but certainly merit further investigation in the future.

The OMI and DOAS SO_2 emission rate time series (Figure 7a) agree reasonably well in shape and general magnitude of daily emission rate, particularly in November. However, several peaks in the DOAS data set are again not matched by corresponding peaks in derived OMI emission rate (most notably, 26 and 29 October and 19 and 25 November). While certain discrepancies have already been identified between satellite-observed data and REMOTE simulated data (such as cloud cover on 7, 8, and 19 October and 7 and 15 November, viewing angle on 18 October, and satellite zoom mode on 19 November), others remain unexplained. Major fluctuations in both emission rate time series in Figure 7 seem to still prevent significant increases in agreement between OMI and DOAS at several intervals of the study period.

Our use of the *model lifetime method* rather than *scene lifetime method* for calculation of derived emission rates does result in improved agreement, however. The percentage difference between mean SO_2 emission rate (October to November 2007) derived from OMI with the *model lifetime method* and the ground-based DOAS data set is 17.6% versus 35.1% between ground-based and satellite emission rates when the *scene*

lifetime method is used (Table 1). Considering 10 day means throughout the study period (Figure 7b), the improvement is less unambiguous, though we note that the derived emission rate data using the *model lifetime method* is either closer to the value of the DOAS data set or else comparable to the value derived in the *scene lifetime method*. The more extensive data set also should make the mean values more representative. The reduced percentage difference is another clear indicator that the use of REMOTE benefits the satellite versus ground-based comparison.

8. Conclusions: The Future of Satellite-Based Volcano Monitoring

Unlocking the potential of satellite-based spectrometers such as OMI for volcano monitoring would constitute a major advance and lead to increases in both temporal and spatial data coverage. Validation of many satellite data products remains sparse, however, and direct comparison of mass loading with ground-based emission rate data is hampered by fundamental differences in how these data are obtained, as well as uncertainty over how truly variation in atmospheric SO_2 mass loadings reflects changing volcanic SO_2 emissions. This study's novel application of the chemistry/transport model REMOTE to the problem of integrating satellite and ground-based measurements of persistent degassing complements other recent work combining satellite observations and model simulations of volcanic emissions.

Our results suggest that at Tungurahua and volcanoes in similar settings, significant variability can arise in daily SO_2 mass loading solely as a result of postemission atmospheric processing of a volcanic SO_2 plume. We explored the relative balance of oxidation of SO_2 to sulphate, dry deposition of SO_2 from the plume, and transport of SO_2 downwind and out of the model domain and found that oxidation accounted for roughly 60% of SO_2 removal and transport the remaining 40%, with dry deposition largely negligible. The mean lifetime for SO_2 over Tungurahua was calculated at ~19.6 h, corresponding to a bulk loss rate of $1.4\times10^{-5}s^{-1}$. It is plausible that this lifetime could be significantly faster in certain circumstances which our simulations could not account for, for example, if high plume ash content were to increase SO_2 reaction or removal. At certain other volcanoes, it is expected that lifetimes could be very different based on differences in environment (e.g., temperature, humidity, and wind speed) or style of degassing (e.g., plume altitude or ash content).

Based on available ground-based SO_2 emission rate data, it seems that variability in SO_2 output at Tungurahua is greater than variability in postemission processing on most days and therefore that SO_2 plume mass should be a good proxy for emission rate. This suggests that the long-term observation data sets from satellite-based instruments like OMI can be useful in providing good first-order constraint on the variability of volcanic emissions in otherwise poorly monitored regions. We cannot rule out the fact, however, that short-lived or seasonal increases in processing extent might cause a shift in this balance, with processing becoming more dominant in modifying SO_2 plume masses. This shift was evident on certain days at Tungurahua, and we emphasize that under different environmental and volcanic conditions the balance could be permanently shifted toward dominance by processing (for example, a volcano emitting roughly constant amounts of SO_2 into a tropical boundary layer atmosphere). In cases such as these, satellite observations of variable mass loading may not be a good proxy for changing emission rates at the source.

Our mean simulated SO_2 mass loadings for October to November 2007 are closer by a factor of 2 to those calculated from OMI data than ground-based measurements of emission rate by DOAS. Our *model lifetime method* derived mean emission rates from OMI are in turn significantly closer to monthly averages calculated from the DOAS data set. This clearly demonstrates that the use of REMOTE can improve satellite-based estimates of SO_2 emission, particularly compared to earlier studies. This is encouraging for the use of satellites in the pursuit of even the broadest estimates of degassing budgets. Quantitative agreement either between OMI SO_2 mass loadings and those simulated by REMOTE or between ground-based UV DOAS measurements of SO_2 emission rate and those derived variously from satellite observations remains limited and highly variable on a daily basis, in part due to large errors on individual data points. We found no dominant control on the agreement between satellite and model data sets, despite considering a large range of parameters. Deconvolving the combined effect of, e.g., cloud cover, wind speed, and viewing geometry remains a key target for further work.

One solution to a limited understanding of daily agreement between the data sets is time-averaging, which we have not explored in any depth here but which merits a brief mention. Smoothing our OMI and

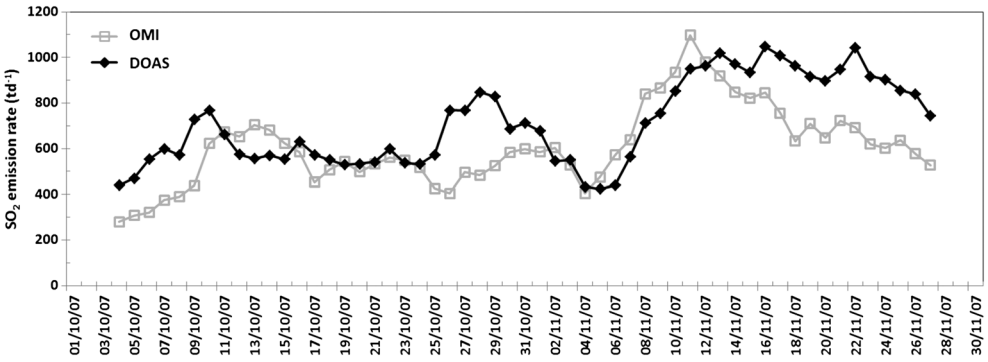

Figure 8. Time series of SO_2 emission rate data sets after smoothing with a 7 day centered moving average. Emission rate data sets are those measured by ground-based UV DOAS spectrometers, and derived from OMI observations using the model lifetime method. The scene lifetime method is too discontinuous to effectively time-average.

DOAS emission rate time series with a 7 day centered moving average reveals a good agreement in trend, with both data sets showing coincident increases and decreases in emission rate (Figure 8). Differences in magnitude are certainly apparent, with DOAS emission rates higher than those of OMI in three clear intervals. Partly, these may be artifacts of the smoothing, close to days where spikes are present in the DOAS time series. During the final 2 weeks of November, however, higher wind speeds (see Figure 6b) could result in shearing or rapid dilution of the plume, thus reducing the SO_2 concentration measurable by OMI.

Such methods clearly offer little to the understanding of daily differences between satellite and ground-based data sets. However, while accurate daily monitoring may be beyond the capability of our current suite of satellite-based instruments, a more limited but nonetheless valuable datastream may still be provided via time-averaging. For example, for placing broad constraint on variability within annual volcanic emissions budgets (e.g., for the climate modeling community), these methods do merit further exploration.

To conclude, this study suggests that where SO_2 lifetime is close to 1 day, satellite-observed SO_2 mass loadings should be a good proxy for volcanic emission strength. On this basis, satellites like OMI could provide a survey of the world's actively degassing volcanoes, with unprecedented spatial and temporal coverage, potentially ranking them in order of persistence and apparent strength of SO_2 output. While the use of chemistry/transport models like REMOTE is time intensive and not suitable for near-real-time monitoring purposes, this work suggests that simulations of postemission processing will help constrain SO_2 lifetime and hence aid the interpretation of satellite-based SO_2 data sets in more quantitative terms, either in understanding the relationship between observed mass loadings and likely emission rates or in deriving emission rates from the observation data set. The development of more sophisticated models with the capability to also include the effects of plume ash content on processing and extended capability for chemical reactions generally is anticipated to provide the groundwork for studies of this kind with much greater scope. Next-generation satellite-based UV spectrometers such as TROPOMI will bring greater sensitivity to volcanic SO_2 in the troposphere [*Veefkind et al.*, 2012]. Reanalysis and reprocessing of observatory data sets, as well as more rigorous operational protocols (e.g., daily plume height measurements, use of locally measured wind speeds instead of model reanalysis data, and further investigation of multiple scattering and light dilution uncertainties) will significantly improve the accuracy and reliability of ground-based measurements. Above all, greater efforts to compare observation data sets between multiple satellite instruments and ground-based monitoring networks would be welcomed.

Acknowledgments

B.T.M. acknowledges funding from the National Centre for Earth Observation, part of the UK's Natural Environment Research Council, and latterly the Deep Carbon Observatory and the Smithsonian Institution. B.T.M., M.E., and T.A.M. are supported by and contribute to the NERC NCEO Dynamic Earth and Geohazards group. S.A.C. acknowledges funding from NASA through grants NNX09AJ40G (Aura Validation), NNX10AG60G (Atmospheric Chemistry Modeling and Analysis Program), and NNX11AF42G (Aura Science Team). J.Y. was funded by the Isaac Newton Trust at the University of Cambridge for the duration of this project. The authors thank Anja Schmidt and two anonymous reviewers for their thorough and constructive comments. We acknowledge the Goddard Earth Sciences Data and Information Services Center for making OMI SO_2 data publicly available.

References

Andres, R., and A. Kasgnoc (1998), A time-averaged inventory of subaerial volcanic sulphur emissions, *J. Geophys. Res.*, *103*(D19), 25,251–25,261.

Arellano, S., M. Hall, P. Samaniego, J.-L. L. Pennec, A. Ruiz, I. Molina, and H. Yepes (2008), Degassing patterns of Tungurahua volcano (Ecuador) during the 1999–2006 eruptive period, inferred from remote spectroscopic measurements of SO_2 emissions, *J. Volcanol. Geotherm. Res.*, *176*, 151–162.

Bani, P., C. Oppenheimer, V. Tsanev, S. Carn, S. Cronin, R. Crimp, J. Calkins, D. Charley, M. Lardy, and T. Roberts (2009a), Surge in sulphur and halogen degassing from Ambrym volcano, Vanuatu, *Bull. Volcanol.*, *71*(10), 1159–1168.

Bani, P., C. Oppenheimer, J. Varekamp, T. Quinou, M. Lardy, and S. Carn (2009b), Remarkable geochemical changes and degassing at Voui crater lake, Ambae Volcano, Vanuatu, *J. Volcanol. Geotherm. Res.*, *188*, 347–357.

Bani, P., C. Oppenheimer, P. Allard, H. Shinohara, V. Tsanev, S. Carn, M. Lardy, and E. Garaebeti (2012), First estimate of volcanic SO_2 budget for Vanuatu island arc, *J. Volcanol. Geotherm. Res.*, *211*, 36–46, doi:10.1016/j.jvolgeores.2011.10.005.

Boichu, M., C. Oppenheimer, V. Tsanev, and P. Kyle (2010), High temporal resolution SO_2 flux measurements at Erebus volcano, Antarctica, *J. Volcanol. Geotherm. Res.*, *190*(3-4), 325–336.

Boichu, M., L. Menut, D. Khvorostyanov, L. Clarisse, C. Clerbaux, S. Turquety, and P.-F. Coheur (2013), Inverting for volcanic SO_2 flux at high temporal resolution using spaceborne plume imagery and chemistry-transport modelling: The 2010 Eyjafjallajökull eruption case-study, *Atmos. Chem. Phys.*, *13*, 8569–8584.

Campion, R., M. Martinez-Cruz, T. Lecocq, C. Caudron, J. Pacheco, G. Pinardi, C. Hermans, S. Carn, and A. Bernard (2012), Space- and ground-based measurements of sulphur dioxide emissions from Turrialba Volcano, *Bull. Volcanol.*, *74*(7), 1757–1770.

Carn, S. (2011), *Omiplot*. [Available at https://vhub.org/resources/682.]

Carn, S., and T. Lopez (2011), Opportunistic validation of sulfur dioxide in the Sarychev Peak volcanic eruption cloud, *Atmos. Meas. Tech.*, *4*, 1705–1712.

Carn, S., and F. Prata (2010), Satellite-based constraints on explosive SO_2 release from Soufrière Hills Volcano, Montserrat, *Geophys. Res. Lett.*, *37*, L00E22, doi:10.1029/2010GL044971.

Carn, S., A. J. Krueger, N. Krotkov, K. Yang, and P. Levelt (2007b), Sulfur dioxide emissions from Peruvian copper smelters detected by the Ozone Monitoring Instrument, *Geophys. Res. Lett.*, *34*, L09801, doi:10.1029/2006GL029020.

Carn, S., A. Krueger, S. Arellano, N. Krotkov, and K. Yang (2008), Daily monitoring of Ecuadorian volcanic degassing from space, *J. Volcanol. Geotherm. Res.*, *176*, 141–150.

Carn, S., A. Krueger, N. Krotkov, K. Yang, and K. Evans (2009a), Tracking volcanic sulphur dioxide clouds for aviation hazard mitigation, *Nat. Hazards*, *51*, 325–343.

Carn, S., J. Pallister, L. Lara, J. Ewert, S. Watt, A. Prata, R. Thomas, and G. Villarosa (2009b), The unexpected awakening of Chaitén Volcano, Chile, *Eos Trans. AGU*, *90*, 205–212, doi:10.1029/2009EO240001.

Carn, S., et al. (2011), In situ measurements of tropospheric volcanic plumes in Ecuador and Colombia during TC4, *J. Geophys. Res.*, *116*, D00J24, doi:10.1029/2010JD014718.

Carn, S., N. Krotkov, K. Yang, and A. Krueger (2013), Measuring global volcanic degassing with the Ozone Monitoring Instrument (OMI), in *Remote Sensing of Volcanoes and Volcanic Processes: Integrating Observation and Modelling*, vol. 380, edited by D. Pyle, T. Mather, and J. Biggs, pp. 229–257, Geol. Soc. Spec. Publ., London.

Dee, D., et al. (2011), The ERA-Interim reanalysis: Configuration and performance of the data assimilation system, *Q. J. R. Meteorol. Soc.*, *137*(656), 553–597.

Delmelle, P. (2003), Environmental impacts of tropospheric volcanic gas plumes, in *Volcanic Degassing*, vol. 213, edited by C. Oppenheimer, D. Pyle, and J. Barclay, pp. 381–399, Geol. Soc. Spec. Publ., London.

Eatough, D., F. Caka, and R. Farber (1994), The conversion of SO_2 to sulphate in the atmosphere, *Isr. J. Chem.*, *34*, 301–314.

Edmonds, M. (2008), New geochemical insights into volcanic degassing, *Phil. Trans. R. Soc. A*, *366*(1885), 4559–4579.

Edmonds, M., R. Herd, B. Galle, and C. Oppenheimer (2003), Automated, high time-resolution measurements of SO_2 flux at Soufriére Hills Volcano, Montserrat, *Bull. Volcanol.*, *65*(8), 578–586.

Ferguson, D., T. Barnie, D. Pyle, C. Oppenheimer, G. Yirgu, E. Lewi, T. Kidane, S. Carn, and I. Hamling (2010), Recent rift related volcanism in Afar, Ethiopia, *Earth Planet. Sci. Lett.*, *292*, 409–418.

Fischer, T. (2008), Volatile fluxes (H_2O, CO_2, N_2, HCl, HF) from arc volcanoes, *Geochem. J.*, *42*, 21–38.

Galle, B., M. Johansson, C. Rivera, Y. Zhang, M. Kihlman, C. Kern, T. Lehmann, U. Platt, S. Arellano, and S. Hidalgo (2010), Network for Observation of Volcanic and Atmospheric Change (NOVAC)—A global network for volcanic gas monitoring: Network layout and instrument description, *J. Geophys. Res.*, *115*, D05304, doi:10.1029/2009JD011823.

Gardine, M., M. West, C. Werner, and M. Doukas (2011), Evidence of magma intrusion at Fourpeaked Volcano, Alaska in 2006–2007 from volcanic emissions and rapid response seismicity, *J. Volcanol. Geotherm. Res.*, *200*, 192–200.

Hall, M., C. Robin, B. Beate, P. Mothes, and M. Monzier (1999), Tungurahua volcano, Ecuador: Structure, eruptive history and hazards, *J. Volcanol. Geotherm. Res.*, *91*, 1–21.

Hansell, A., and C. Oppenheimer (2004), Health hazards from volcanic gases: A systematic literature review, *Arch. Environ. Health*, *59*(12), 628–639.

Haywood, J., et al. (2010), Observations of the eruption of the Sarychev volcano and simulations using the HadGEM2 climate model, *J. Geophys. Res.*, *115*, D21212, doi:10.1029/2010JD014447.

Heard, I., A. Manning, J. Haywood, C. Witham, A. Redington, A. Jones, L. Clarisse, and A. Bourassa (2012), A comparison of atmospheric dispersion model predictions with observations of SO_2 and sulphate aerosol from volcanic eruptions, *J. Geophys. Res.*, *117*, D00U22, doi:10.1029/2011JD016791.

Ichoku, C., and Y. Kaufman (2005), A method to derive smoke emission rates from modis fire radiative energy measurements, *IEEE Trans. Geosci. Remote Sens.*, *43*, 2636–2649.

IGEPN (2007a), *Resumen Mensual Actividad del Volcán Tungurahua, Octubre del 2007*, Instituto Geofísica de la Escuela Politécnica Nacional.

IGEPN (2007b), *Resumen Mensual Actividad del Volcán Tungurahua, Noviembre del 2007*, Instituto Geofísica de la Escuela Politécnica Nacional.

IGEPN (2007c), *Resumen Semanale Actividad del Volcán Tungurahua*, pp. 40–48, Instituto Geofísica de la Escuela Politécnica Nacional.

IPCC (2007), Climate change 2007: The physical science basis, in *Contribution of Working Group I to the Fourth Assessment Report of the Intergovernmental Panel on Climate Change*, edited by S. Solomon et al., 996 pp., Cambridge Univ. Press, Cambridge, U. K., and New York.

Kern, C. (2009), Spectroscopic measurements of volcanic gas emissions in the ultraviolet wavelength region, PhD thesis, Univ. Heidelberg, Heidelberg.

Kern, C., T. Deutschmann, L. Vogel, M. Wöhrbach, T. Wagner, and U. Platt (2010), Radiative transfer corrections for accurate spectroscopic measurements of volcanic gas emissions, *Bull. Volcanol.*, *72*, 233–247.

Kern, C., T. Deutschmann, C. Werner, A. Sutton, T. Elias, and P. Kelly (2012), Improving the accuracy of SO_2 column densities and emission rates obtained from upward-looking UV-spectroscopic measurements of volcanic plumes by taking realistic radiative transfer into account, *J. Geophys. Res.*, *117*, D20302, doi:10.1029/2012JD017936.

Langmann, B. (2000), Numerical modelling of regional scale transport and photochemistry directly together with meteorological processes, *Atmos. Environ.*, *34*(21), 3585–3598.

Langmann, B., M. Hort, and T. Hansteen (2009), Meteorological influence on the seasonal and diurnal variability of the dispersion of volcanic emissions in Nicaragua: A numerical model study, *J. Volcanol. Geotherm. Res.*, *182*, 34–44.

Langmann, B., K. Zakšsek, and M. Hort (2010), Atmospheric distribution and removal of volcanic ash after the eruption of Kasatochi volcano: A regional model study, *J. Geophys. Res.*, *115*, D00L06, doi:10.1029/2009JD013298.
Levelt, P., G. van den Oord, M. Dobber, A. Mëlkki, H. Visser, J. de Vries, P. Stammes, J. Lundell, and H. Sari (2006a), The ozone monitoring instrument, *IEEE Trans. Geosci. Remote Sens.*, *44*(5), 1093–1100.
Levelt, P., E. Hilsenrath, G. Leppelmeier, G. van den Oord, P. Bhartia, J. Tamminen, J. de Haan, and J. Veefkind (2006b), Science objectives of the ozone monitoring instrument, *IEEE Trans. Geosci. Remote Sens.*, *44*(5), 1199–1208.
Lopez, T., S. Carn, C. Werner, D. Fee, P. Kelly, M. Doukas, M. Pfeffer, P. Webley, C. Cahill, and D. Schneider (2013), Evaluation of Redoubt volcano's sulfur dioxide emissions by the ozone monitoring instrument, *J. Volcanol. Geotherm. Res.*, *259*, 290–307.
Marmer, E., and B. Langmann (2005), Impact of ship emissions on the Mediterranean summertime pollution and climate: A regional model study, *Atmos. Environ.*, *39*(26), 4659–4669.
Mather, T., D. Pyle, V. Tsanev, A. McGonigle, C. Oppenheimer, and A. Allen (2006), A reassessment of current volcanic emissions from the Central American arc with specific examples from Nicaragua, *J. Volcanol. Geotherm. Res.*, *149*, 297–311.
McCormick, B., M. Edmonds, T. Mather, and S. Carn (2012), First synoptic analysis of volcanic degassing in Papua New Guinea, *Geochem. Geophys. Geosyst.*, *13*, Q03008, doi:10.1029/2011GC003945.
McCormick, B., M. Edmonds, T. Mather, C. Hayer, R. Campion, H. Thomas, and S. Carn (2013), Volcano monitoring applications of the Ozone Monitoring Instrument (OMI), in *Remote Sensing of Volcanoes and Volcanic Processes: Integrating Observation and Modelling*, vol. 380, edited by D. Pyle, T. Mather, and J. Biggs, pp. 259–291, Geol. Soc. Spec. Publ., London.
McGonigle, A., P. Delmelle, C. Oppenheimer, V. Tsanev, T. Delfosse, G. Williams-Jones, K. Horton, and T. Mather (2004), SO_2 depletion in tropospheric volcanic plumes, *Geophys. Res. Lett.*, *31*, L13201, doi:10.1029/2004GL019990.
Mellor, B., and T. Yamada (1974), A hierarchy of turbulence closure models for planetary boundary layers, *J. Atmos. Sci.*, *31*, 1791–1806.
Merucci, L., M. Burton, S. Corradini, and G. Salerno (2011), Reconstruction of SO_2 flux emission chronology from space-based measurements, *J. Volcanol. Geotherm. Res.*, *206*, 80–87.
Mori, T., H. Shinohara, K. Kazahaya, J. Hirabayashi, T. Matsushima, T. Mori, M. Ohwada, M. Odai, H. Iino, and M. Miyashita (2013), Time-averaged SO_2 fluxes of subduction-zone volcanoes: Example of a 32-year exhaustive survey for Japanese volcanoes, *J. Geophys. Res. Atmos.*, *118*, 8662–8674, doi:10.1002/jgrd.50591.
Nadeau, P., and G. Williams-Jones (2009), Apparent downwind depletion of volcanic SO_2 flux lessons from Masaya Volcano, Nicaragua, *Bull. Volcanol.*, *71*, 389–400.
NASA (2008), *Sulphur dioxide from Noril'sk, Russia: Image of the day*. [Available at http://earthobservatory.nasa.gov/IOTD/view.php?id=36063.]
NASA (2010), *Introducing the A-train*. [Available at http://nasa.gov/mission_pages/a-train/.]
O'Dowd, C., et al. (2012), The Eyjafjallajökull ash plume—Part 2: Simulating ash cloud dispersion with REMOTE, *Atmos. Environ.*, *48*, 143–151.
Oppenheimer, C., P. Francis, and J. Stix (1998), Depletion rates of sulfur dioxide in tropospheric volcanic plumes, *Geophys. Res. Lett.*, *25*(14), 2671–2674.
Oppenheimer, C., B. Scaillet, and R. Martin (2011), Sulphur degassing from volcanoes: Source conditions, surveillance, plume chemistry and Earth system impacts, *Rev. Mineral. Geochem.*, *73*, 363–421.
Palma, J. L. (2013), *Wind reanalysis*. [Available at http://vhub.org/resources/windre/.]
Pfeffer, M., B. Langmann, and H.-F. Graf (2006), Atmospheric transport and deposition of Indonesian volcanic eruptions, *Atmos. Chem. Phys.*, *6*, 2525–2537.
Pfeffer, M., B. Langmann, A. Heil, and H. Graf (2012), Numerical simulations examining the possible role of anthropogenic and volcanic emissions during the 1997 Indonesian fires, *Air Qual. Atmos. Health*, *5*(3), 277–292.
Robock, A. (2000), Volcanic eruptions and climate, *Rev. Geophys.*, *38*, 191–219.
Rodríguez, L., I. Watson, M. Edmonds, G. Ryan, V. Hards, C. Oppenheimer, and G. Bluth (2008), SO_2 loss rates in the plume emitted by Soufriére Hills volcano, Montserrat, *J. Volcanol. Geotherm. Res.*, *173*, 135–147.
Saxena, P., and C. Seigneur (1987), On the oxidation of SO_2 to sulfate in atmospheric aerosols, *Atmos. Environ.*, *21*(4), 807–812.
Schmidt, A., K. Carslaw, G. Mann, A. Rap, K. Pringle, D. Spracklen, M. Wilson, and P. Forster (2012), Importance of tropospheric volcanic aerosol for indirect radiative forcing of climate, *Atmos. Chem. Phys.*, *12*, 7321–7339.
Seigneur, C., and P. Saxena (1988), A theoretical investigation of sulphate formation in clouds, *Atmos. Environ.*, *22*(1), 101–115.
Siebert, L., and T. Simkin (2002), *Volcanoes of the World: An Illustrated Catalog of Holocene Volcanoes and their Eruptions*. [Available at http://volcano.si.edu.]
Smolarkiewitz, P. (1983), A simple positive definite advection scheme with small implicit diffusion, *Mon. Weather Rev.*, *111*, 479–486.
Sparks, R., J. Biggs, and J. Neuberg (2012), Monitoring volcanoes, *Science*, *335*(6074), 1310–1311.
Spinei, E., S. Carn, N. Krotkov, G. Mount, K. Yang, and A. Krueger (2010), Validation of ozone monitoring instrument SO_2 measurements in the Okmok volcanic cloud over Pullman, WA, July 2008, *J. Geophys. Res.*, *115*, D00L08, doi:10.1029/2009JD013492.
Steffke, A., D. Fee, M. Garces, and A. Harris (2010), Eruption chronologies, plume heights and eruption styles at Tungurahua volcano: Integrating remote sensing techniques and infrasound, *J. Volcanol. Geotherm. Res.*, *193*, 143–160.
Stockwell, W., P. Middleton, J. Chang, and X. Tang (1990), The second generation regional acid deposition model: Chemical mechanism for regional air quality monitoring, *J. Geophys. Res.*, *95*, 16,343–16,367.
Symonds, R., W. Rose, G. Bluth, and T. M. Gerlach (1994), Volcanic gas studies methods, results, and applications, *Rev. Mineral.*, *30*, 1–66.
Theys, N., et al. (2013), Volcanic SO_2 fluxes derived from satellite data: A survey using OMI, GOME-2, IASI and MODIS, *Atmos. Chem. Phys.*, *13*, 5945–5968.
Thomas, H., I. Watson, S. Carn, A. Prata, and V. Realmuto (2011), A comparison of AIRS, MODIS and OMI sulphur dioxide retrievals in volcanic clouds, *Geomatics, Nat. Hazards and Risk*, *2*(3), 217–232.
Tiedtke, M. (1989), A comprehensive mass flux scheme for cumulus parameterisation in large-scale models, *Mon. Weather Rev.*, *117*, 1778–1800.
Veefkind, J., et al. (2012), TROPOMI on the ESA Sentinel-5 Precursor: A GMES mission for global observations of the atmospheric composition for climate, air quality and ozone layer applications, *Remote Sens. Environ.*, *120*, 70–83.
Wallace, P., and M. Edmonds (2011), The sulphur budget in magmas: Evidence from melt inclusions, submarine glasses, and volcanic gas emissions, *Rev. Mineral. Geochem.*, *73*(1), 215–246.
Williams-Jones, G., K. Horton, T. Elias, H. Garbeil, P. Mouginis-Mark, A. Sutton, and A. Harris (2006), Accurately measuring volcanic plume velocity with multiple UV spectrometers, *Bull. Volcanol.*, *68*(4), 328–332.
Yang, K., N. Krotkov, A. Krueger, S. Carn, P. Bhartia, and P. Levelt (2007), Retrieval of large volcanic SO_2 columns from the Aura Ozone Monitoring Instrument: Comparison and limitations, *J. Geophys. Res.*, *112*, D24S43, doi:10.1029/2007JD008825.